UNIV RSITY OF R ADING
D PARTM NT OF MATH MATICS

HIGHER ORDER GODUNOV BLACK-OIL SIMULATIONS FOR COMPRESSIBLE FLOW IN POROUS MEDIA

by

DWIN MICHA L DICKS

This thesis is submitted for the degree of
Doctor of Philosophy

MARCH 1993

Numerical reservoir simulation is an important area of research within the oil industry. An accurate prediction of the performance of a reservoir under a recovery strategy is needed to assess the optimum oil recovery, and hence to determine the economics of the project.

Acknowledgements

I would like to express many thanks to my supervisor Dr Pete Sweby for his ideas, encouragement and patience during the writing of this thesis.

I also thank Dr Mike Christie of B.P. Research Sunbury for his guidance of the research and much advice.

I would also like to thank the Postgraduates who have been at the Mathematics Department over the last three years for making my stay so enjoyable.

I also thank the members, past and present, of Dr Mike Christies's research team at Sunbury for their help during my visits, especially Dr Mark Mansfield for many hours spent in obtaining the results from the reservoir simulation code VIP.

In addition I acknowledge the Science and ngineering Research Council for the award of a CAS studentship for the period of my studies, and the British Petroleum Company plc for their financial support.

Ch pter 1

Introduction

1.1 Oil Reservoir Engineering

Oil reservoir engineering encompasses the processes of reservoir characterisation, mathematical modelling of the physical processes involved in reservoir fluid flow, and finally the numerical prediction of a given fluid flow scenario. The basic problem associated with oil recovery involves the injection of fluid or combinations of fluids and/or chemicals into the reservoir via injection wells to force as much oil as possible towards and hence out of production wells. Accurate prediction of the performance of a given reservoir under a particular recovery strategy is essential for an estimation of the economics, and hence risk, of the oil recovery project. Therefore a large amount of research, and money, is directed towards the above processes, by the oil industry.

The reservoir characterisation process provides the physical parameters, such as size, resident fluid and rock composition and properties, which are needed by the mathematical model. Given the physical parameters, the mathematical model describes the fluid flow with a set of partial differential equations and other relations, which are derived from physical principles. The resulting set of partial differential equations are too complex, for most realistic reservoir fluid flow models, to be solved by analytic methods. Therefore numerical methods are called upon to perform this task, resulting in the field of numerical reservoir simulation. Design of oil recovery strategies is heavily influenced by numerical simulation, by simulating various injection strategies the optimum recovery technique can

be assessed. Simulation is also useful for aiding understanding of the physical processes involved in reservoir fluid flow.

An oil reservoir can be described as a region of porous rock containing mixtures of oil, gas and water trapped in the rock pores, surrounded above, below, and to the sides by impermeable rock. The available pore volume in the rock, in which the fluid resides, is given by the rock porosity which is defined as the rock pore volume divided by the bulk volume. Another important parameter characterising reservoir rock is the permeability which is a measure of how readily fluid flows through the rock under the influence of the forces causing the flow. Oil reservoirs are located in many parts of the world both inshore and offshore, for example land based reservoirs in the United States and reservoirs under the North Sea. Reservoirs vary in size, usually being very large in area and can be in the region of 200 feet thick, resulting in very large field scale simulation operations. Many different types of rock may exist in the reservoirs, with the porosity of most commercially productive reservoirs being 10-25 , and with rock permeability ranging from 0.5 to 3500 milliDarcy's [14]. In practice reservoirs are not homogeneous in nature, the main reason for this being the variation of the permeability field. Fractures in the rock and shales (impermeable laminates) also add to the complexity of the simulation project.

Three types of oil recovery technique exist and are referred to as primary, secondary and tertiary (also known as enhanced oil recovery OR). In the primary process, oil is forced out of the reservoir, at a production well, by the naturally prevailing pressure gradients, but is only effective at producing a few percent of the original oil in the reservoir, before the pressure gradients subside. The pressure gradient, which forces the oil towards the production well, may be restored by injection of fluid such as water, known as waterflooding, to help force more oil to the production well. The technique of injecting water (and/or gas) to restore the pressure gradients in the reservoir is known as secondary recovery.

The efficiency of wateflooding may be improved by lowering the water-oil

A mobility ratio M of greater than unity is referred to as unfavourable since the water is more mobile than the oil and can 'finger' through the oil zone, a process known as viscous fingering. This results in a reduced oil recovery efficiency, but may be improved by decreasing the ratio M by increasing the water viscosity. This can be accomplished by addition of chemicals such as polymers to the water, the displacement of oil by water then occurring in a piston-like way. Application of secondary recovery techniques can result in a 20-50 recovery of oil [14], depending on the oil and reservoir properties.

Tertiary recovery (OR) involves one of a number of procedures, such as injection of chemicals, miscible displacement processes and thermal recovery methods, which are described in [14]. These methods are designed to increase the recovery from reservoirs previously depleted by secondary recovery techniques. Chemical and miscible displacement processes are used to recover low viscosity oils by controlling the mobility ratio or decreasing the interfacial tension between the oil and the other fluids. The thermal methods of steamflooding and combustion techniques are used to recover high viscosity oils, with the heat transferred to the oil reducing its viscosity causing it to flow more easily. In this thesis we consider injection of water and immiscible gas and therefore consider secondary recovery techniques only.

1.2 Mathematical Modelling of Reservoir Fluid Flow

A number of mathematical models exist for the description of fluid flow in oil reservoirs. These can be divided into categories as to whether the fluid flow is considered to be compressible or incompressible and whether the fluid components are immiscible or miscible. A fluid component is deemed compressible if the volume it occupies is dependent on its pressure. The compressibility associated with the reservoir rock may also be modelled. Fluid components are considered miscible if they are able to mix in all proportions without any interface forming between them. The physical parameters of the resulting fluid mixture, for example viscosity and density, are then obtained from a relation involving the

individual fluid component parameters and are known as mixing laws. This is in contrast to immiscible fluids in which different phases exist which exhibit distinct

has been presented by Trangenstein and Bell in [46] and is the formulation of the flow equations used in this thesis. This method decouples the parabolic and hyperbolic behaviour by a linearisation of the volume balance equation to form the parabolic equation for pressure, however this introduces a 'volume error discrepancy' which is a consequence of the linearisation and indicates that the volume balance equation is not exactly satisfied.

An alternative compressible fluid flow model exists, called the compositional model, which is used when the modelling capabilities of the Black-Oil model

1.3 Numerical Methods for Reservoir Simulation

numerical diffusion, resulting in the smearing of shock fronts over many grid cells. Whereas the classical second order methods, although increasing the resolution of the shocks suffer from spurious oscillation in their vicinity. Hence work in the oil industry on high resolution (second order accurate), oscillation free Total Variation Diminishing (TVD, see [24]) numerical schemes was undertaken. A number of TVD flux-limiter type methods had been independently proposed, outside the oil industry, by a number of authors, for example Roe [34] and Van Leer [50]. However explicit and implicit TVD flux-limiter schemes have been developed for use in the oil industry by, for example, Blunt and Rubin [7] and Rubin and dwards [36]. These methods are based on the types of numerical fluxes typically used in the oil industry, rather than using the Lax Wendroff flux, as in [34] and [50]. Originally reservoir simulation codes only achieved first order accuracy in space and time, but with advent of the flux-limiter schemes in [7] and [36] can now achieve second order accuracy whilst being free of numerical oscillations, i.e. TVD. Flux Corrected Transport (FCT), another high resolution non-oscillatory method [8, 9, 56], has also been applied, but to the more restricted circumstances of incompressible miscible flow.

There has also been a recent interest in the application of Godunov type methods to reservoir simulation. These methods, originally developed by Godunov [20], have undergone extensive development and are applied to a wide range of problem areas. Solutions of Riemann problems are central to these types of scheme and the analytic framework of the conservtoedulGaM4 IUhemeNcrporated into the numerica sheme. In thlGaM[)'-3UtheslGaM[)'-3UwN'I-(UeNM[)'-3UapplyNM[)'-3UtheN present in the system of conservation -4l[UNM4, specifically -ocal -inear degeneracies and eigenvector deficiencies which the Black-Oil model possesses, and therefore is particularly suited to numerical reservoir simulation. The scheme re-ies on a knowledge of the characteristic structure of the conservt[3]-IU-4l[UedNM4]N[3]-IUto]N[3]-IUacN'F

Bell [46], we show results of three of these simulations. We also present results of a 2-D Areal problem, which have not previously been seen in the literature. In this chapter we also investigate the accuracy of the Higher Order Godunov method when applied to degenerate systems, by comparing the numerical results of 3-phase incompressible Buckley-Leverett simulations with the corresponding analytic solutions which we construct. The incorporation of source terms in 1 and 2 dimensions, to model injection of fluid into, and production of fluid from

Chapter 2

Hyperbolic Conservation Laws

2.1 Introduction

In this chapter we review some of the theory and nomenclature, associated with hyperbolic conservation laws, which we use throughout this thesis. Firstly an indication of how hyperbolic conservation laws are derived and characterised is given. Particular attention is given to systems that exhibit two types of degen-

2.2 Derivation

posed. The differential equation along with the initial condition is said to hold on a region Ω, the boundary of which is denoted by Ω. Boundary conditions on Ω may be needed depending on the structure of the problem, i.e. whether there is inflow, outflow or reflection from the boundaries.

2.3 haracterisation

The equation (2.2.1) is said to be in conservation form, with the quasi-linear form being given by

$$\text{—} + \text{——} = 0$$

where — is an matrix called the Jacobian matrix. If — is a function of and only then the conservation laws are termed linear, whereas if — is also a function of then we have a non-linear system. The system (2.2.1) is termed hyperbolic if all the eigenvalues of the Jacobian matrix are real. If the eigenvalues are also distinct then the system is referred to as strictly hyperbolic. If this is the case then the eigenvectors and eigenvalues of the Jacobian satisfy

$$\text{——} = \Lambda$$

where Λ is a real diagonal matrix and a real non-singular matrix. The entries of Λ are termed characteristic wavespeeds and the columns of , denoted by , the characteristic directions. A loss of strict hyperbolicity occurs when two or more wavespeeds coincide at a point, which is referred to as an umbilic point.

A particular eigenvalue and its corresponding eigenvector define a characteristic field of the system. The characteristic field is said to be genuinely non-linear if

$$\text{——} = 0$$

—

In this thesis we consider systems of conservation laws which exhibit certain pathologies in their wave structure as previously mentioned. In particular we consider systems with the following two degeneracies, namely those which exhibit local linear degeneracy and eigenvector deficiencies in the wavefields. A local linear degeneracy occurs at a specific value of $\mathbf{U}$ for which the genuine non-linearity condition fails. An eigenvector deficiency arises when two or more eigenvalues coincide and their corresponding eigenvectors are parallel. Other degeneracies are also possible such as elliptic, parabolic and rotational but we do not consider these.

2.4 Analytic Solutions

2.4.1 The Weak Form

The differential form of the conservation laws preclude discontinuous solutions, however the problems of interest to us, namely the simulation of flow in porous media, typically exhibit discontinuous solutions hence we need to consider the weak form of the conservation laws. The weak form is an integral formulation and hence discontinuous solutions are admitted. It is obtained by multiplying the conservation laws by a smooth test function ϕ which has compact support, i.e. is zero outside of some finite interval, and integrating over the region, resulting in

$$\int_0^\infty \int_{-\infty}^\infty [\phi_t \mathbf{U} + \phi_x \mathbf{F}(\mathbf{U})]\, dx\, dt = -\int_{-\infty}^\infty \phi(x,0)\mathbf{U}(x,0)\, dx.$$

For more details see Smoller [41] or any other standard text on hyperbolic conservation laws. The conservation laws are then satisfied in the sense of distributions and discontinuous solutions are now allowed since the act of integrating by parts moves the derivatives onto the test function. Admission of discontinuous solutions has a consequences in that weak solutions are non-unique, hence a way of selecting the physically correct solution is required.

2.4.2 Entropy Conditions

The way in which a discontinuity is determined as being physically correct is if it satisfies a condition known as an ntropy Condition. The entropy condition

requires that the physically meaningful solution to the conservation laws is the limit of the solution to a modified differential equation, with an infinitesimal amount of diffusion, namely

$$\mathbf{U}_t + \mathbf{F}_x = \epsilon \mathbf{U}_{xx},$$

as the diffusion tends to zero, i.e. $\epsilon \downarrow 0$. This condition is thought, see for example Trangenstein [49], to be reasonable when considering reservoir flow problems, particularly so when diffusive forces such as capillary pressure and mixing are ignored. This is because enforcement of the entropy condition ensures that the solutions to the conservation laws are related to more realistic flow models which do include diffusive forces.

Work by Oleinik [31] and Lax [28] has provided straightforward quantitative versions of the entropy condition. Oleinik showed that the scalar Riemann problem has an admissible shock from u^L to u^R if and only if

$$\frac{f(u) - f(u^L)}{u - u^L} \geq \sigma \geq \frac{f(u) - f(u^R)}{u - u^R},$$

for all u between u^L and u^R and termed this condition , where σ is the shock speed and is given by

$$\sigma = \frac{f(u^L) - f(u^R)}{u^L - u^R}.$$

Condition applies to both convex and non-convex scalar conservation laws, whereas Lax showed that the convex problem has an admissible weak shock if the shock speed σ satisfies

$$a(u^L) > \sigma > a(u^R),$$

where $a(u)$ $(= f'(u))$ is the wavespeed of the scalar conservation law. This second condition states that the characteristics should go into the shock as time progresses. For convex f Oleinik's condition reduces to that of Lax. A similar condition for systems is also due to Lax and is expressed by

$$\lambda_k(\mathbf{U}^L) > \sigma > \lambda_k(\mathbf{U}^R),$$

where λ_k denotes one of the characteristic wavespeeds of the system, and is only valid for genuinely non-linear fields. If satisfied for a particular k the discontinuity

is referred to as a shock. In the case of characteristic fields which are not genuinely non-linear another entropy condition is required. This extended entropy condition is due to Liu [30] and is given by

$$(\quad) \qquad (\quad)$$

and is less restrictive than the Lax condition for genuinely non-linear fields by allowing equality of the shock speed with one of the wavespeeds.

The Riemann problem is defined as the initial value problem (2.2.1) with a single discontinuity in the initial data,

$$(\quad 0) = \begin{array}{ll} & \text{if} \quad 0 \\ & \text{if} \quad 0 \end{array}$$

where and are constant states to the left and right respectively of the initial discontinuity at $= 0$. The Riemann problem is very important in the theory of hyperbolic conservation laws since it serves as a component of a number of numerical schemes.

The solution to the Riemann problem is composed of two types of elementary waves, termed shocks and rarefactions, usually connected by constant states. Another type of wave termed a contact discontinuity may also arise. A shock is a discontinuity that satisfies an appropriate entropy condition and travels with the Rankine-Hugoniot shock speed which is given below. An expression for the speed of a propagating shock can be obtained from the weak form of the conservation laws, and is given by the following well known Rankine-Hugoniot jump condition

$$= \frac{(\quad) \qquad (\quad)}{}$$

The contact discontinuity is not a valid shock, but is a valid discontinuity and may arise if one of the characteristic fields is linearly degenerate. In this case the wavespeeds on both sides of the discontinuity are equal and hence the discontinuity moves with speed equal to the wavespeed.

A rarefaction is a smoothly varying solution which is a function of the similarity variable only. The following characterisation of rarefaction solutions exists, a rarefaction is defined by

$$- = \quad (\quad)$$

$$(\quad) \qquad (\quad) \qquad (\quad)$$

where is any state on the rarefaction wave and and are states to the left and right of the wave.

Classical hyperbolic theory, see Lax [28], states that for an system the Riemann problem solution is composed of distinct waves connecting to . For a strictly hyperbolic system these waves can only be connected by constant states, but for a system that exhibits local linear degeneracies, rarefaction-shock compound waves become a possibility, see Liu [30]. For example a 1 rarefaction may be connected to a 1 shock, in fact the two waves must be of the same family because at the connection point the fastest wavespeed in the rarefaction must be equal to the first characteristic speed to the left of the shock. Shock-rarefaction compound waves are also a possibility. However, some types of compound waves are precluded, depending on the number of components in the system and the degree of the flux function, for example see Schaeffer and Shearer [38]. Also, at points where strict hyperbolicity fails, transitional

2.5 Numerical Solutions

We shall consider conservative difference schemes for numerically solving the system (2.2.1), as we want to retain the conservation property of the equations. This is important because not only do we maintain conservation, but an important theorem of Lax and Wendroff [29] will then apply. This theorem states that if the numerical scheme is convergent then it converges to a weak solution of the conservation laws (2.2.1). As a consequence shock wave solutions will satisfy the Rankine-Hugoniot relation for the shock speed, so that shocks will appear in the correct locations. This type of difference scheme may be derived by integrating the conservation laws over a box in space defined by [_ _] [ ] and applying the Gauss divergence theorem, which results in

$$= \frac{\Delta}{\Delta}(\quad \bar{} \quad \bar{}) \qquad (2\ 5\ 2)$$

where we have used standard notation and Δ = _ _ and Δ = . The quantity is an integral averaged value of over the interval, i.e.

$$= \frac{1}{\Delta} \quad \bar{} \quad (\ \Delta \quad \Delta \ )$$

The $\bar{}$ is termed the numerical flux and is defined by

$$\bar{} = \frac{1}{\Delta} \quad (\ (\quad _ \ )) \ _$$

where _ is the unit outward normal to the relevant face of the space-time box.

If the fluxes $\bar{}$ in the finite difference update (2.5.2) are functions of quantities at the current time level then the resulting scheme is termed explicit. In this case all the quantities on the right hand side of (2.5.2) are known and hence the

sides of (2.5.2) are functions of . In general implicit methods are more

were present in the original equation together with spatial derivatives only. The elimination method should not use the original partial differential equation as its solution will not satisfy the finite difference equations. Instead the result of the Taylor series expansion of the finite difference approximation should itself be manipulated by applying — and — operators and taking linear combinations of these forms with the original expansion to remove the required derivatives. The resulting modified equation will have infinitely many terms but in practice only the lowest order terms need be considered as these describe the dominant behaviour. For example when a first order finite difference method is used to approximate the solution to the linear advection equation analysis shows that the modified equation is actually of the form

$$+ \quad =$$

where the term is a diffusion term. Hence the reason for first order methods suffering from large doses of numerical diffusion. Similarly with second order methods, the modified equation looks like

$$+ \quad =$$

with the term being a dispersive term. This term gives rise to the dispersive ripples in the Lax-Wendroff and Warming and Beam schemes.

Two examples of scalar first order schemes are the upwind scheme and the

$$- \qquad —$$
$$-$$
$$—$$

states to the left and right of the discontinuity at = , where specifies the speed of the discontinuity. Godunov's method takes the cell edge flux to be

$$\bar{}_{-} = \quad (\quad (\qquad\qquad 0))$$

---

where $TV(u^n)$ is the total variation of the solution at time level n and is defined by

$$TV(u^n) = \sum_k |u^n_{k+1} - u^n_k|.$$

The total variation is an important property of a numerical scheme which can be used to prove convergence of a scheme, and also ensures that oscillations cannot appear in the solution.

The concept of a TVD scheme is essentially one-dimensional although a definition of the total variation of the solution to the two-dimensional conservation laws of the form

$$u_t + f_x + g_y = 0,$$

has been given by Goodman and LeVeque [23]. The total variation is defined by the sum of the variations in both coordinate directions and is given by

$$TV(u^n) = TV_x(u^n) + TV_y(u^n) = \Delta y \sum_{j,k} |u^n_{j+1,k} - u^n_{j,k}| + \Delta x \sum_{j,k} |u^n_{j,k+1} - u^n_{j,k}|.$$

Goodman and LeVeque [23] showed that any scheme in two-dimensions which satisfies the TVD criteria (2.5.5) must be only first order accurate. However, when most 1-D TVD methods are applied in 2-D they usually work well in practice. Second order accuracy is maintained on smooth solutions and no oscillatory behaviour is observed, despite the fact that the scheme is not strictly TVD.

Other types of non-oscillatory scheme, which are not TVD, have been developed for multidimensional linear advection by for example Roe and Sidilkover [35]. Their scheme is termed an Optimum Positive Linear Scheme for linear advection. The coefficients of such schemes are positive quantities, which defines a positive scheme, and are optimum in the sense that the truncation error is minimised. This is accomplished by a particular choice of coefficients, subject to the positivity condition. xtension of numerical schemes to model multidimensional flow is usually made on a dimension by dimension basis, i.e. dimensionally splits schemes, which will be outlined later. However this approach is reported in the literature to give poor results if the flow is unsteady or not aligned with the grid directions, hence the development of the Positive schemes. These schemes are said to be the multidimensional equivalent of simple upwinding and in 2-D have been shown to be about 4 times less dissipative than the dimensionally split

schemes, and permit time steps that can be greater by a factor of 2. Roe and Sidil

It is well known that the Lax-Wendroff scheme is not TVD due to the spurious oscillations it produces near shocks, as previously mentioned. This can be remedied by adding only a limited amount of the antidiffusive flux to the first order scheme by introducing a flux-limiter ϕ_j

$$u_j^{n+1} = u_j^n - \nu\Delta u_{j-\frac{1}{2}} - \Delta_-(\phi_j \frac{1}{2}(1-\nu)\Delta u_{j+\frac{1}{2}}),$$

where ϕ_j is a function ϕ of a parameter r_j which is taken to be a ratio of consecutive gradients, i.e.

$$r_j = \frac{\Delta u_{j-\frac{1}{2}}}{\Delta u_{j+\frac{1}{2}}}.$$

The limiter function ϕ is then chosen such that the limited antidiffusive flux is maximised subject to the TVD constraint. Details of this procedure for the linear and non-linear cases can be found in Sweby [45]. The result of the analysis by Sweby can be shown graphically, i.e. a region in ϕ, r space in which the limiter must lie to give a second order TVD scheme, which is given by the shaded area in Figure 2.1. For example $\phi(r) = 1$ reverts the scheme back to Lax-Wendroff and

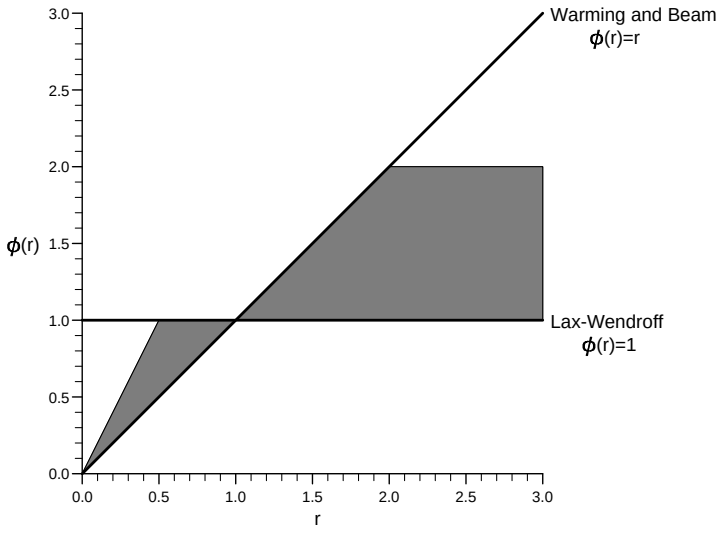

Figure 2.1: The second order TVD region, also indicating the limiter functions ϕ corresponding to the Lax-Wendroff and Warming and Beam schemes.

$\phi(r) = r$ gives the scheme of Warming and Beam. As can be seen from Figure 2.1 these two lines do not lie entirely within the TVD region hence explaining the non TVD property of these two classical schemes. The following conditions also exist on the limiter function, firstly if $r \leq 0$ then $\phi = 0$ so that the sign

cell interface, whereas the Higher Order Godunov scheme uses a fuller description of the Riemann problem.

The general principle is as follows. The piecewise constant approximation, denoted by ( ) say, of the solution at the current time level is given in each grid cell = [_ _] by

$$( ) = \quad \text{for}$$

The piecewise linear approximation ( ) is constructed in each cell by the interpolant of

$$+\frac{1}{2}\Delta \quad \text{and} \quad \frac{1}{2}\Delta \tag{2 5 6}$$

i.e. is given by

$$( ) = + ( ) \text{ for} \tag{2 5 7}$$

The slopes must be chosen such that the integral of the piecewise linear approximation over each cell is the same as with = 0 and the total variation of the resulting profile, is not increased. Hence the piecewise linear representation maintains conservation as cell averages are preserved. The slope can be given the 2nlyfluxU(+fi2nlyfuncffDGG,2(Ufi2UL.ffD MU(U(+fiItl(1(+=lffDG+2(Ufi2nly=fionffs2(Ufi2

_ _

_ _

Ch pter 3

he Bl ck-Oil Fluid Flow E u tions

3.1 Introduction

The Black-Oil model is the industry standard mathematical model most often used in petroleum reservoir simulation. It assumes that the fluid components are immiscible and includes compressibility and the general mass transfer effects between the phases that are needed to model primary (pressure depletion) and secondary (water injection) recovery. The particular form of the model we are using in our reservoir computations was developed byaclrangenstein and Bellac[46] and is one of a number of formulations of the 'Black-Oil' type which are distinct from another class of model termed the compositional model. A compositional model [47] quite similar to the Black-Oil model46] has also been developed by rangenstein and Bell.

main difference between the two approaches are that Black-Oil models consider general fluid components, i.e. collections of individual chemical species (hydrocarbons) which are then termed either oil or gas, whereas the compositional models consider individual hydrocarbon species such as ethane and butane

Therefore a more accurate description of hydrocarbon phase behaviour is provided, but the resulting phase equilibrium problem is very complex. Compositional models are used when the modelling capabilities of Black-Oil models are

extra computational expense of the iterative techniques needed to solve phase equilibrium along with the larger systems of conservation laws, because of the consideration of individual species, limits their applicability.

Reservoir fluid flow equations exhibit both hyperbolic and parabolic behaviour, for instance fronts separating different fluid states move at a finite speed of propagation whereas pressure effects are quickly felt throughout the reservoir. Both of these types of behaviour can be treated by a fully implicit discretisation. However, to effectively treat both types of behaviour present in the flow equations, different types of numerical procedure are required for each and so a splitting of the flow equations into a system of hyperbolic conservation laws and a parabolic pressure equation is used. In addition, implicit discretisations of the unsplit equations typically use large amounts of numerical diffusion, providing further reason for use of the sequential (or split) strategy.

In our computations with the Black-Oil model we follow Trangenstein and Bell and use the Higher Order Godunov method to discretise the hyperbolic part of the flow equations. This numerical scheme is able to address the problems associated with eigenvector deficiency and local linear degeneracy which are present in the Black-Oil model. The pressure equation is discretised using a Backward- uler (implicit) approach.

Sequential methods were first proposed by Sheldon et al. [39] and Stone and Garder [43] around thirty years ago. These early and some subsequent formulations contained certain anomalies, for instance the hyperbolic and parabolic parts were not properly separated. Further developments were made, and in 1986 Bell, Shubin and Trangenstein [5] presented a new sequential method to model two-phase, two-component fluid flow. This formulation is based on conservation of mass of the fluid components and does not have the consequences of a 'volume error discrepancy' which is present in their later work. The volume error discrepancy indicates the extent to which the volume balance equation is not satisfied and is described in Section 3.4. This later work by Trangenstein and Bell [46] models three-phase, three-component fluid flow, and is the formulation we are working with. It should be noted that the form of the Black-Oil model used in

development. For a description of the formulations that are used, see Aziz and Settari [1].

The fluid flow equations are derived from four main principles which are used to derive most isothermal porous media flow models. These are:

i) Phase equilibrium - determines how the components combine to form phases,

ii) The equation of state - requires that the fluid fills the pore volume,

iii) Darcy's law for the volumetric flow rates,

iv) Mass conservation equations for each component.

The flow equations are formulated sequentially, therefore they cannot be satisfied exactly at each step of the computation, and so some incompatibility is introduced. Phase equilibrium, Darcy's law and the component conservation laws are satisfied exactly but the equation of state is linearised so that it is only satisfied approximately. This splitting of the flow equation is termed a 'volume-discrepancy splitting'.

In the next four sections of this chapter we describe the formulation, and the equations that result, of the four main principles used to derive the mathematical model. Then we summarise the sequential formulation in broad terms and mention the consequences of the splitting of the flow equations and the resulting volume error discrepancy. In the last section we describe the parameters of the model we used for our reservoir computations.

3.2 Thermodynamic Equilibrium

The fluid in the reservoir is considered to be composed of three components, oil, gas, and water. These are the separations the fluid chooses at surface temperatures and pressures. However to reach phase equilibrium at reservoir conditions these components combine to form at most three phases, liquid, vapour and aqua.

are conserved by mass, thus it is necessary to determine how the mass of each component is apportioned into the phases. This phase equilibrium problem can be expressed as follows: given the pressure p and the vector $\mathbf{n} = [n_o, n_g, n_w]^T$ of mass component densities, find the matrix

$$N = \begin{bmatrix} n_{ol} & n_{ov} & 0 \\ n_{gl} & n_{gv} & n_{ga} \\ 0 & 0 & n_{wa} \end{bmatrix}$$

of component densities in each of the phases, subject to the mass balance condition

$$\mathbf{n} = N\mathbf{e},$$

where $\mathbf{e}$ is a vector of one's of the appropriate length. Thus it can be seen from the definition of N that there is a restriction on the way the components are allowed to mix in the phases, i.e. oil may be allowed in the liquid and vapour phases, gas in all three phases and water in the aqueous phase only. Oil and water do not mix and steam is not treated due to the isothermal nature of the model. At this point there is not enough information to solve the phase equilibrium problem, this extra information is provided in the next two sections.

3.2.2 Mass Transfer and Phase Equilibrium

A principal component is associated with each phase, oil with the liquid phase, gas with the vapour phase and water with the aqueous phase. The amount of each component in each phase is related to the amount of the principal component in that phase by the ratio matrix R. When all three phases are formed R is given by

$$R = \begin{bmatrix} 1 & R_v & 0 \\ R_l & 1 & R_a \\ 0 & 0 & 1 \end{bmatrix} = N_{\ N},$$

where $_N$ is the diagonal part of N. For example the solution gas ratio defined by

$$R_l = n_{gl}/n_{ol},$$

to volatilise into vapour, then it is possible that no liquid is formed and the vapour phase is undersaturated. In the present work neither , or are identically equal to zero therefore both types of undersaturation are possible. Analysis of undersaturated flow, see [46], shows that at most one phase can be missing due to undersaturation. Therefore both types of undersaturated flow occurring simultaneously would be impossible. The possibility also exists of a phase being missing due to the principal component associated with that phase being missing. If this is the case the fluid will still be termed saturated as the phase will not be missing due to mass transfer effects. For example if no oil is present then the liquid phase will not be formed.

When the vapour phase is missing the physical meaning of the negative vapour component of is that the fluid prestn Ao7icalGigither tnat theTinent pr-As7VOHG 9H80)O

case of the vapour phase being undersaturated, Q and $\mathbf{q}$ are given by

$$Q = \begin{bmatrix} 0 & 0 \\ 1 & 0 \\ 0 & 1 \end{bmatrix} \quad , \quad \mathbf{q} = \begin{bmatrix} 1 \\ 0 \\ 0 \end{bmatrix},$$

and if the liquid phase is undersaturated

$$Q = \begin{bmatrix} 1 & 0 \\ 0 & 0 \\ 0 & 1 \end{bmatrix} \quad , \quad \mathbf{q} = \begin{bmatrix} 0 \\ 1 \\ 0 \end{bmatrix}.$$

Throughout this chapter, quantities denoted with an overbar refer to the reduced matrix or vector in the undersaturated case.

The solution to phase equilibrium is then given by

$$N = \overline{R}\,\overline{\ }_N Q^T.$$

In the case of the liquid phase being undersaturated the matrix N is given by

$$N = \begin{bmatrix} n_o & 0 & 0 \\ \overline{R}_l n_o & 0 & \overline{R}_a n_w \\ 0 & 0 & n_w \end{bmatrix},$$

i.e. all the oil is contained in the liquid phase and the gas present is dissolved in both the liquid and aqueous phases. When the vapour phase is undersaturated the matrix N is given by

$$N = \begin{bmatrix} 0 & n_o & 0 \\ 0 & n_g - R_a n_w & R_a n_w \\ 0 & 0 & n_w \end{bmatrix}.$$

Here all the oil has volatilised into the vapour phase and the gas in the vapour phase is equal to the total amount of gas less the gas dissolved in the aqueous phase. In both cases of undersaturation, as well as saturated flow, all of the water must be in the aqueous phase.

In the case of undersaturated flow an undersaturation parameter ω is used to develop the flow equations and becomes one of the dependent variables. In the case of an undersaturated liquid ω becomes the bubble point pressure and in the case of undersaturated vapour ω is the volatile oil ratio.

In this section we examine the compressibility of the reservoir fluids and describe their effect on the phase volumes.

Fluid compressibility is defined by

$$= \frac{1}{} = \frac{1}{}$$

where is the volume of the fluid and is its density. The negative sign is needed since compressibilities are defined as positive numbers. The compressibilities of oil and water are considered constant, typical values would be, for oil 2 0 10 psi and for water 3 0 10 psi . Gas compressibility is usually considered a function of pressure, and for this work ranges from 9 0 10 psi at 1000 psi to 3 0 10 psi at 3000 psi. Here psi refers to the unit of pressure in pounds per square inch.

The small compressibilities of oil and water, along with the relatively high compressibility of gas, and the swelling effects caused by gas dissolving in liquid lead to important volume changes at reservoir pressures. The Black-Oil model incorporates these volume changes by relating the volumes of each of the phases to the amount of the principal component in that phase. To quantify this relationship is defined to be the diagonal matrix of iphase. effAtif)ARG H8Ads7C

no mass transfer is assumed to have a small compressibility in that as pressure increases the liquid phase volume decreases. If we then allow mass transfer so that gas, which is more compressible than oil, is allowed to dissolve in the oil, then for pressures below the bubble point, increases in pressure cause more gas to dissolve and the phase volume then increases, and to a greater extent than with no mass transfer. Above the bubble point pressure the liquid phase is assumed slightly compressible. These effects can be described by,

$$(\quad) = \begin{cases} 1 & \text{if} \quad = 0 \\ 1 + & \text{if} \\ \text{————} & \text{if} \end{cases}$$

Here is the compressibility of the pure oil component and is the compressibility of the liquid phase, i.e. oil containing dissolved gas. Analogous formulas

—

— —

With this definition, the saturations sum to one even if the volume balance equation is not satisfied. It should be noted that must be considered distinct from because of the volume error discrepancy associated with this formulation of the flow equations. However in the case of no volume error discrepancy when = 1 the vectors and are identical.

Relative permeability describes how the presence of each phase adversely affects the flow of the other phases and are non-negative functions of the saturations . Due to the complex interaction of the phases with the rock pore space the dependence of the relative permeabilities on the rock and fluid properties is not fully understood. However it is known that as the saturation of a phase approaches zero, its mobility must tend to zero implying its relative permeability must vanish. In reality a phase will become immobile before its saturation reaHfiA)'fieGfiH8OAish.arati7

=
hp4Ah-m.i7GRF8Rfftfl

3.4 Equation of State

When satisfied exactly, the equation of state (or volume balance equation) states that the fluid fills the rock pore volume, i.e.

$$\mathbf{e}^T\mathbf{u} = 1, \tag{3.4.4}$$

where as usual $\mathbf{e}$ is the vector of one's. The extent to which this equation is not satisfied, i.e. the sum of the phase volumes is not equal to the pore volume, is termed the volume error discrepancy and is given by

$$\mathbf{e}^T\mathbf{u} - 1.$$

In the sequential formulation it is not possible to satisfy all of the fluid flow constraints simultaneously and so equation (3.4.4) is linearised to form an equation for pressure. Performing a Taylor's series linearisation about time level t gives

$$\mathbf{e}^T\mathbf{u}\Big|_{t+\Delta t} \approx \mathbf{e}^T\mathbf{u}\Big|_t + \Delta t\mathbf{e}^T\frac{\partial\mathbf{u}}{\partial t}\Big|_t. \tag{3.4.5}$$

It is assumed that we have a volume error discrepancy at time level t, i.e. $\mathbf{e}^T\mathbf{u}\Big|_t = 1$, and we wish to calculate pressure at the advanced time $t+\Delta t$ such that there is no volume error, i.e. $\mathbf{e}^T\mathbf{u}\Big|_{t+\Delta t} = 1$. Applying these assumptions and since $\mathbf{u}$ is a function of $\mathbf{n}$ and p, equation (3.4.5) becomes

$$\frac{1 \quad \mathbf{e}^T\mathbf{u}}{\Delta t} \quad \mathbf{e}^T\frac{\partial\mathbf{u}}{\partial p}\frac{\partial p}{\partial t} + \mathbf{e}^T\frac{\partial\mathbf{u}}{\partial\mathbf{n}}\frac{\partial\mathbf{n}}{\partial t}.$$

Multiplication by the porosity ϕ and use of the mass conservation laws to replace the time derivative of $\mathbf{n}$ results in the following equation for pressure

$$\frac{(\mathbf{e}^T\mathbf{u} \quad 1)\phi}{\Delta t} \quad (\phi\mathbf{e}^T\frac{\partial\mathbf{u}}{\partial p} + \mathbf{e}^T\frac{\partial\mathbf{u}}{\partial\mathbf{n}}\mathbf{n}\frac{\partial\phi}{\partial p})\frac{\partial p}{\partial t} \quad \mathbf{e}^T\frac{\partial\mathbf{u}}{\partial\mathbf{n}}\frac{\partial}{\partial x}(N \quad {}_u^{-1}v).$$

First degree homogeneity properties of the phases are now used to simplify the term multiplying $\frac{\partial p}{\partial t}$. Firstly the matrix of partial phase volumes is computed, which in the saturated case is

$$\frac{\partial\mathbf{u}}{\partial\mathbf{n}} = BT.$$

Post multiplying this by N gives

$$\frac{\partial\mathbf{u}}{\partial\mathbf{n}}N = BTN = BR^{-1}R \quad {}_N = \quad {}_u.$$

This implies that

$$\frac{\partial \mathbf{u}}{\partial \mathbf{n}}\mathbf{n} = \mathbf{u},$$

which says that each phase volume $\mathbf{u}$ is a homogeneous function of the first degree in the fluid composition $\mathbf{n}$. An identical result also holds in the undersaturated case.

The pressure equation can now be written in the general form

$$c\frac{\partial p}{\partial t} + \mathbf{w}^T \frac{\partial}{\partial x}(\mathbf{f}v_T + \mathbf{g}\tau) = q, \tag{3.4.6}$$

with the total velocity v_T being given by

$$v_T = [-\frac{\partial p}{\partial x} + \gamma]\tau, \tag{3.4.7}$$

where the coefficients c, $\mathbf{w}$, $\mathbf{f}$, $\mathbf{g}$, γ, q and τ depend on the pressure p and component density $\mathbf{n}$. For completeness we define them here

$$c = \phi \mathbf{e}^T \frac{\partial \mathbf{u}}{\partial p} - \mathbf{e}^T \mathbf{u} \frac{\partial \phi}{\partial p},$$

$$\tau = \mathbf{e}^T L \mathbf{e} \kappa \quad , \quad \gamma = \frac{\mathbf{e}^T L \boldsymbol{\rho}}{\mathbf{e}^T L \mathbf{e}} g \frac{\partial d}{\partial x}$$

$$\mathbf{f} = N \quad {}_u^{-1} L \mathbf{e} \frac{1}{\mathbf{e}^T L \mathbf{e}}$$

$$\mathbf{g} = N \quad {}_u^{-1} L \boldsymbol{\rho} g \frac{\partial d}{\partial x} \frac{1}{\mathbf{e}^T L \mathbf{e}} - \mathbf{f}\gamma$$

$$\mathbf{w}^T = \mathbf{e}^T \frac{\partial \mathbf{u}}{\partial \mathbf{n}} \quad , \quad q = \frac{(\mathbf{e}^T \mathbf{u} - 1)\phi}{\Delta t}.$$

For a more detailed discussion on the pressure equation, including its numerical solution, see Section 3 of [49].

3.4.1 Analysis of the Pressure Equation

To examine the character of (3.4.6) we need to examine the coefficient c of $\frac{\partial p}{\partial t}$ and the coefficient of $\frac{\partial^2 p}{\partial x^2}$ which is obtained after substitution of (3.4.7) into (3.4.6) and is given by

$$-\mathbf{w}^T \mathbf{f} \tau = -\mathbf{e}^T L \mathbf{e} \kappa,$$

since $\mathbf{w}$ and $\mathbf{f}$ satisfy $\mathbf{w}^T \mathbf{f} = 1$. It is known that pressure effects within the reservoir are of parabolic nature for compressible fluid flow, so we need to ensure

that the differential equation (3.4.6) is of parabolic type. The transmissibility is positive, hence the coefficient of — is negative, and therefore for (3.4.6) to be parabolic is required to be negative. Now, as pressure increases the rock occupies a smaller volume hence porosity is a non-decreasing function of pressure,— 0. Therefore for to be negative the inequality — 0 is required which is the condition of negative total fluid compressibility. This is guaranteed by placing restrictions on the formation volume factors and ratios , namely

— 0

with a more complicated condition in the undersaturated case, see [46].

3.5 onservation of Mass

The mass of each fluid component is required to be conserved. The matrix represents the density of each fluid component in each phase, hence the conservation of mass equations are

—( ) + —( ) = 0 (3 5 8)

The flux function = can also be expressed as = , which is the form that will be used in the characteristic analysis. Here the vector of Darcy phase velocities is written in terms of the total velocity , i.e. in the form (3.3.3). The flux is therefore a function of , and , hence in quasi-linear form we have

— + —— = —— —— —— —— (3 5 9)

where is a gravitational term, namely

= —

The term — is only nonzero if the porous medium is hetero48is=s=sS)ffiO0)siGH r3 +G8ars

—

—

has real eigenvalues for all values of $\mathbf{n}$. We also need to compute the eigenvalues and right eigenvectors of H to provide information about the structure of the wave fields, which will be needed by the numerical method that we use to solve the conservation laws. Both p and v_T are considered to be independent of $\mathbf{n}$ for the purpose of the characteristic analysis since the volume balance equation (3.4.4) is not enforced in the sequential formulation. To calculate the hyperbolic wavespeeds we must divide the eigenvalues by the porosity ϕ since it multiplies the time derivative of $\mathbf{n}$ in the quasi-linear form of the conservation laws.

3.5.1 Characteristic Analysis

For saturated flow a similarity transformation and eigenvector deflation is used to derive the matrix of eigenvectors X, of H. The component derivative of the flux vector $\mathbf{h}$ is given by

$$\frac{\partial \mathbf{h}}{\partial \mathbf{n}} = RB^{-1}\frac{\partial \mathbf{v}}{\partial \mathbf{n}},$$

since only $\mathbf{v}$ is a function of $\mathbf{n}$. xpansion of $\frac{\partial \mathbf{v}}{\partial \mathbf{n}}$ using the chain rule and further manipulation yields

$$H\mathbf{e}^T\mathbf{u} = RB^{-1}\frac{\partial \mathbf{v}}{\partial \mathbf{s}}[I - \mathbf{s}\mathbf{e}^T]BR^{-1}.$$

Therefore it can be seen that $H\mathbf{e}^T\mathbf{u}$ is similar to the matrix

$$V = \frac{\partial \mathbf{v}}{\partial \mathbf{s}}[I - \mathbf{s}\mathbf{e}^T],$$

which is the same matrix that appears in the characteristic analysis of the 3 phase incompressible Buckley-Leverett model [49]. Therefore the similarity transformation defined by

$$H\mathbf{e}^T\mathbf{u} = M_1 V M_1^{-1}, \quad \text{where} \quad M_1 = RB^{-1},$$

can be considered to map from component densities to saturations. The matrix V can now used to deduce one of the eigenvalues of the system because of the relation

$$\mathbf{e}^T V = 0,$$

which arises because the total fluid velocity is independent of $\mathbf{s}$. Thus $\mathbf{e}$ is a left eigenvector of V with eigenvalue zero. This eigenvector is then used to deflate V

as follows:

$$M\ VM \quad = \quad \begin{matrix} 0 & 0 \\ & C \end{matrix} \quad ,$$

where

$$M \ = \ \begin{matrix} 1 & \\ 0 & I \end{matrix} \quad ,$$

C is a 2 2 matrix given by

$$C = [\ 0 \quad I\ ] \ \frac{\partial}{\partial} \qquad \qquad ,$$
$$I$$

and is a 2 vector defined by

$$= \quad C[\ 0 \quad I\ ] \ .I$$

We therefore now have a block-eigenproblem to solve with the remaining 2 eigenvalues of being eigenvalues of matrix , i.e.

$$\begin{matrix} 0 & 0 \\ & \end{matrix} \quad \begin{matrix} 1 & 0 \\ & \end{matrix} \quad = \quad \begin{matrix} 1 & 0 \\ & \end{matrix} \quad \begin{matrix} 0 & 0 \\ 0 & \Lambda \end{matrix}$$

This block-eigenproblem yields four equations which are $0 = 0$ twice, $=$ Λ and the relation $+$ $= 0$ which we need to solve for vector . If we put $=$ then this last relation can be re-expressed, so that we need to solve for where

$$\Lambda \quad = \qquad \qquad (3\ 5\ 10)$$

It is assumed that a real, non-singular matrix and a real diagonal matrix Λ can be found so that

$$= \quad \Lambda$$

The right eigenvectors of are then given by the columns of

$$= \quad \begin{matrix} 1 & \\ 0 & \end{matrix} \quad \begin{matrix} 1 & 0 \\ 0 & \end{matrix} \quad \begin{matrix} 1 & 0 \\ & \end{matrix}$$

and the corresponding full matrix of eigenvalues is then

$$\Lambda = \begin{matrix} 0 & 0 \\ 0 & (\text{——})\Lambda \end{matrix}$$

To summarise we have $HX = X\Lambda$ where X and Λ are given above.

When one of the fluid components and hence phases is missing in saturated flow, the corresponding row and column of the Jacobian matrix $\frac{\partial \mathbf{h}}{\partial \mathbf{n}}$, and hence the matrix $\frac{\partial \mathbf{v}}{\partial \mathbf{s}}$, are both zero. This means that the similarity transformation defined by the matrix M_1 cannot be used because $(RB^{-1})(BR^{-1}) \neq I$, hence the analysis must be reformulated. The remedy is straightforward because we can work with the Jacobian matrix H directly, since it has a zero row, instead of deflating matrix V. We still have the zero eigenvalue, and can proceed with the block-eigenproblem as before.

The two non-trivial eigenvalues obtained from matrix C, i.e. the entries of Λ_c, are the same as the eigenvalues from the 3 phase Buckley-Leverett problem. This shows that the hyperbolicity of the system is inherited from the relative permeability model and not the compressibility and mass transfer effects which complicate the Black-Oil model.

In the case of undersaturated flow a similarity transformation of H is also used to find the eigenvectors and eigenvalues, with the eigenvectors given by

$$X = \begin{bmatrix} \overline{R}\,\overline{B}^{-1} & \mathbf{q} \end{bmatrix} \begin{bmatrix} X_{\overline{v}} & 0 \\ 0 & 1 \end{bmatrix} \begin{bmatrix} I & -\mathbf{a} \\ 0 & 1 \end{bmatrix}.$$

The analysis proceeds as before, again reducing to a block-eigenproblem. Here $\mathbf{q}$ is a constant vector dependent on which phase is missing, and the vector $\mathbf{a}$ solves

$$X_{\overline{v}}\,((\frac{1}{\mathbf{e}^T\mathbf{u}})\Lambda_{\overline{v}}\mathbf{a} - \mathbf{a}\lambda) = \overline{B}\,\overline{T}H\mathbf{q}.$$

This auxiliary equation, which we need to solve for $\mathbf{a}$, corresponds to (3.5.10) in the saturated flow analysis. $X_{\overline{v}}$ and $\Lambda_{\overline{v}}$ are given by

$$X_{\overline{v}} = \begin{bmatrix} \mathbf{s}_* & -1 \\ \mathbf{s}_a & 1 \end{bmatrix} \quad , \quad \Lambda_{\overline{v}} = \begin{bmatrix} 0 & 0 \\ 0 & \frac{\partial v_a}{\partial s_a} - \frac{\partial v_a}{\partial s_*} \end{bmatrix},$$

where s_* is the saturation of the other existing phase. The full matrix of eigenvalues is then given by

$$\Lambda = \begin{bmatrix} (\frac{1}{\mathbf{e}^T\mathbf{u}})\Lambda_{\overline{v}} & 0 \\ 0 & \lambda \end{bmatrix},$$

3.6 Sequential Formulation

The idea behind the splitting of the equations into a pressure equation and a system of conservation laws is that, over some time interval, we first solve for pressure with the composition fixed and compute a total velocity. We then solve for the new composition with pressure and total velocity fixed, i.e. with the latest values of and . Thus the sequential method is based on alternately freezing

a severe restriction on their time step due to stability considerations, i.e. Δ should be of the order $(\Delta\ )$. For this reason the reservoir simulation community have used implicit discretisations of the pressure equation so that this restrictive stability condition does not apply, as most implicit methods are unconditionally stable. This motivation for use of an implicit method does not carry over to the solution of the conservation laws. This is because the stability condition for hyperbolic conservation laws is less restrictive, i.e. Δ should be of the order Δ . Also implicit discretisations of conservation laws typically are more diffusive than explicit methods. For these reasons an explicit method has usually been used to discretise the hyperbolic conservation laws arising in the sequential formulation of the Black-Oil model. However there are cases when an implicit method is desirable, for instance, when the fronts in the problem travel at much slower speeds bexp9e p9eusuallyesphasAw7fiFHfi3vlapAconservnAa7CHRfi9HSAt0fi)F2-pfi1AeSA

3.7 2- omponent 2-Phase Black-Oil Model

$$= \begin{cases} 0\ 35 & \text{if aqua is saturated} \\ 0\ 35(1 + 6\ 78 \quad 10 \quad (\qquad)) & \text{if aqua is undersaturated.} \end{cases}$$

We recall the component density vector has the units of standard cubic feet per reservoir cubic foot. This results in the formation volume factors having the units of reservoir cubic feet per standard cubic foot, and these functions are given by

$$(\qquad) = \begin{cases} 1 \quad 2\ 31 \quad 10 & \text{if} \quad (\ ) = 0 \\ 1 + 1\ 5 \quad 10 & \text{if liquid is saturated (} \qquad \text{)} \\ \text{———————} & \text{if liquid is undersaturated (} \qquad \text{)} \end{cases}$$

$$(\quad \bar{} \quad) = \begin{cases} \text{———} & \text{if vapour is saturated} \\ \text{———} + \bar{} [\text{———} \quad \text{———}] & \text{if vapour is undersaturated} \end{cases}$$

$$(\qquad) = \begin{cases} 1 \quad 6\ 78 \quad 10 & \text{if} \quad (\ ) = 0 \\ 1 \quad 3\ 0 \quad 10 & \text{if aqua is saturated (} \qquad \text{)} \\ \text{———————} & \text{if aqua is undersaturated (} \qquad \text{)} \end{cases}$$

The definitions of and when and are zero respectively are provided, even though we have = 0, because and may be forced to zero when the relevant fluid component is missing.

From the definition of the aqueous formation volume factor above, it can be seen that the compressibility of water ( ) is 6 78 10 psi . The value of

used in the computations, unless otherwise stated, were

$$\boldsymbol{\rho} = \begin{bmatrix} 52.787 \\ 0.05154 \\ 62.3967 \end{bmatrix},$$

with the units of lb ft^{-3}, and are only needed when gravitational effects are included.

Ch pter

he Higher Order Godunov Scheme

4.1 Introduction

The Black-Oil model described in the previous chapter exhibits both lack of strict hyperbolicity and points of local linear degeneracy. Therefore to effectively treat such a system of conservation laws requires a numerical method that can handle

We now review the Higher Order Godunov method [2, 10] for degenerate systems of 1-dimensional conservation laws. In multi-dimensions a central concern is the choice of the unsplit versus split methodology, this will be discussed later

4.2 Details of the Scheme

right states, that are used to compute a numerical flux, are second order approximations at the half time level and the cell edge then the overall scheme will be second order accurate. Of course this is only in regions of smooth flow, the monotonisation process lowers the order of accuracy at discontinuities. The numerical flux at the cell edge is computed by solving a local Riemann problem there. ven in problems for which the Riemann problems are well understood analytically, it is usually more computationally efficient to introduce approximations, for example see Roe [33]. In any case there is not much point in solving the Riemann problem to a greater accuracy than that of the underlying discretisation. This idea is central to the approximate Riemann problem solution given in [2], which proceeds by computing a generalisation of the ngquist-Osher numerical flux for systems.

The Higher Order Godunov scheme, in the 1-dimensional case, can be considered as a 5-step procedure:

1. Beginning with the piecewise constant approximation , compute 'centred', 'left' and 'right' slopes, whilst maintaining conservation.
2. 'Limit' the slopes using monotonicity criteria, again whilst maintaining conservation. This provides a piecewise linear discontinuous approximation to the solution at time .
3. Trace along characteristics, using a Taylor series extrapolation, to derive left and right states at grid cell interfaces at time + -Δ . It is possible that the traced states are unphysical, if this is the case the physical cell centred value is used instead.
4. Solve the Riemann problem with these left and right states.

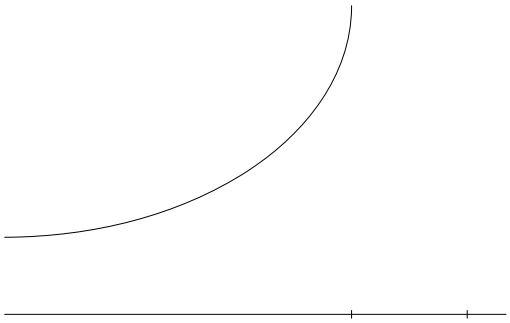

, the more numerical diffusion added into the scheme, with $= 0$ reducing the scheme to first order. There are three important criteria which the above slope limiting formula obeys, these are

1. If the cell average is a local extremum then the slope is set to zero,
2. If the sign of a slope is different to that of either of its neighbours then it is set to zero, i.e. the local trend in slope signs is maintained,
3. The linear profile should not take values beyond those of the neighbouring cell averages.

However, additional limiting is required when local linear degeneracies and eigenvector deficiencies are detected amongst the . A sufficient modification given by Trangenstein [49], when a local linear degeneracy is detected would be to set $= 1\ 5$ for that particular wavemode. Local linear degeneracies are associated with shock-rarefaction compound waves and are detected by testing for a change in sign of spatial differences of the wavespeeds, i.e.

$$(\qquad)(\qquad) \quad 0$$

If this test is satisfied at grid pointongst

of the jump

$$\frac{1}{2}(\qquad\qquad)$$

corresponding to

$$+ \tag{4 2 5}$$

involves an eigenvector deficiency, i.e. and are nearly parallel. To detect for such an eigenvector deficiency the following test given in [2] may be used

$$0\ 1$$

This test estimates whether it is possible for both of the wavespeeds to coincide in a neighbourhood of the state at which the eigenvectors are evaluated. The are called structural coefficients and represent the gradient of the eigenvalue with respect to the conserved variables in the direction of a particular eigenvector, and are defined by

$$= (\qquad)$$

If this test is satisfied then the wavemodes and are assumed to involve an eigenvector deficiency. To ensure the slope limiting process does not introduce instabilities it is necessary to treat the entire jump corresponding to (4.2.5) as one wave because individual components of the jump are badly behaved. This means

$$- \quad - \quad -$$

We now focus on the calculation of the traced left and right states used to determine the numerical flux. The monotonised slopes defined by (4.2.3) are used to construct time-centred left and right states at the cell edges. Values in cell j are used to compute $\mathbf{U}_{j+-}^{n+-,L}$ and $\mathbf{U}_{j--}^{n+-,R}$, the computation being based on a Taylor series expansion about the cell centre, with the quasi-linear form of the hyperbolic equations used to replace the temporal derivatives of $\mathbf{U}$. The left state to second order accuracy in both space and time is given by

$$\begin{aligned} \mathbf{U}_{j+-}^{n+-,L} &= \mathbf{U}_j^n + \frac{\Delta x}{2}\mathbf{U}_{x,j} + \frac{\Delta t}{2}\mathbf{U}_{t,j} \\ &= \mathbf{U}_j^n + \frac{\Delta x}{2}\mathbf{U}_{x,j} \quad \frac{\Delta t}{2}\mathbf{F}_{x,j} \\ &= \mathbf{U}_j^n + (\frac{\Delta x}{2}I \quad \frac{\Delta t}{2}H_j)\ \mathbf{U}_{x,j}, \end{aligned} \tag{4.2.6}$$

where H is the Jacobian matrix $\frac{\partial \mathbf{F}}{\partial \mathbf{U}}$.

For linear problems (4.2.6) can be used to compute a left traced state by replacing $\mathbf{U}_x$ with the monotonised slope approximation (4.2.1). A right traced state is calculated with a similarly derived formula. For nonlinear problems however, (4.2.6) must be modified to disregard components of $\mathbf{U}_x$ corresponding to waves that do not propagate towards the correct cell edge, i.e. for nonlinear problems different characteristics may propagate towards both cell edges, but we only want to use information traveling to the left to calculate the left state and information traveling to the right to calculate the right state, due to the upwind nature of the scheme. This subtraction of unwanted information is accomplished by multiplication of the second order terms in (4.2.6) by the characteristic projection operators defined by

$$P^{\pm} = R\Lambda^{\pm}R^{-1},$$

where R is a matrix with columns $\mathbf{r}_k$ and $\Lambda^{\pm}$ is a diagonal matrix with

$$\Lambda_{kk}^{\pm} = \frac{1}{2}(1 \quad \text{sign}(\lambda_k)),$$

where if we have $\lambda_k = 0$ then we take $\Lambda_{kk} = 1$. This procedure is redundant in the linear case but has been reported by Collela [10] to lead to a more robust algorithm for strongly nonlinear problems.

Formally the left and right states at cell edge + – are then given by

$$\begin{matrix} - \\ - \end{matrix} = + \frac{1}{2} \quad (\quad \frac{\Delta}{\Delta} \quad) \Delta$$

$$\begin{matrix} - \\ - \end{matrix} = \quad \frac{1}{2} \quad (\quad + \frac{\Delta}{\Delta} \quad) \Delta$$

(We note The first order Godunov scheme may be recovered by setting the Δ 's

$$\begin{matrix} - \\ - \end{matrix} \quad - \quad \text{—}$$

$$\begin{matrix} - \\ - \end{matrix} \quad - \quad \text{—}$$

$$\begin{matrix} - & - \\ - & - \end{matrix} \quad \text{—}$$

$$\begin{matrix} - & - \\ - & - \end{matrix} \quad \text{—}$$

In the general case of finite amplitude jumps, the phase space solution of the Riemann problem takes the form

$$\mathbf{U}^R - \mathbf{U}^L = \sum_{k=1}^{K} \alpha_k \mathbf{R}_k,$$

where $\mathbf{R}_k$ is a generalised eigenvector that represents the net change along Γ_k, and which is normalised to be of unit length.

The approximate phase space solution is therefore a decomposition of the jump from $\mathbf{U}^L$ to $\mathbf{U}^R$ into K jumps corresponding to each of the wave modes. To approximate this decomposition a simple phase space solution is used, as was recommended in [2] for problems involving flow in porous media. We calculate an expansion state as the average of the left and right states

$$\overline{\mathbf{U}} = \frac{1}{2}(\mathbf{U}^L + \mathbf{U}^R),$$

and then evaluate the generalised eigenvectors at this expansion state

$$\overline{\mathbf{R}}_k = \mathbf{r}_k(\overline{\mathbf{U}}),$$

so that $\overline{\mathbf{R}}_k$ becomes an approximation to $\mathbf{R}_k$. If we expand $\mathbf{U}^R - \mathbf{U}^L$ in terms of the $\overline{\mathbf{R}}_k$ we have,

$$\mathbf{U}^R - \mathbf{U}^L = \sum_{k=1}^{K} \overline{\alpha}_k \overline{\mathbf{R}}_k, \tag{4.2.7}$$

so that $\overline{\alpha}_k$ approximates α_k. It is also assumed that the $\overline{\mathbf{R}}_k$ are orientated so that the $\overline{\alpha}_k$ are positive. The approximate path in phase space, for example a 2-system is shown in Figure 4.3.

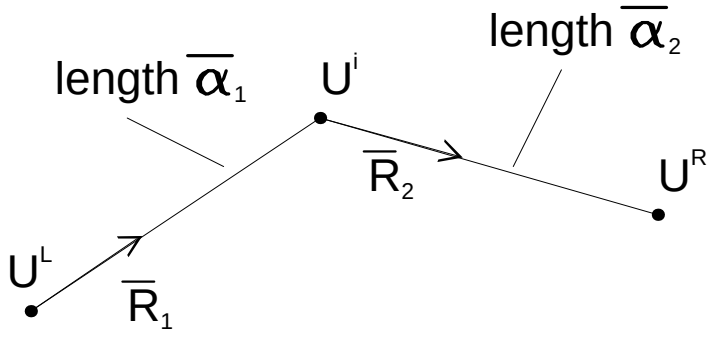

Figure 4.3: The path in phase space, taken by the Riemann problem solution, connecting the left and right states at the cell interface.

The intermediate state shown in Figure 4.3 given by

$$= \quad + - —$$

The numerical flux is then written as a flux at a reference state plus integral correction terms which were constructed to be of dissipative form. Firstly to determine this reference state a mean speed

$$= \frac{(\ (\quad) \quad (\quad)) \ (\quad)}{} \tag{4 2 8}$$

is calculated and the reference state is then defined by

$$= \quad \text{if} \quad 0$$

$$= \quad \text{otherwise}$$

—

– – —

– – —

– –

—

–

—

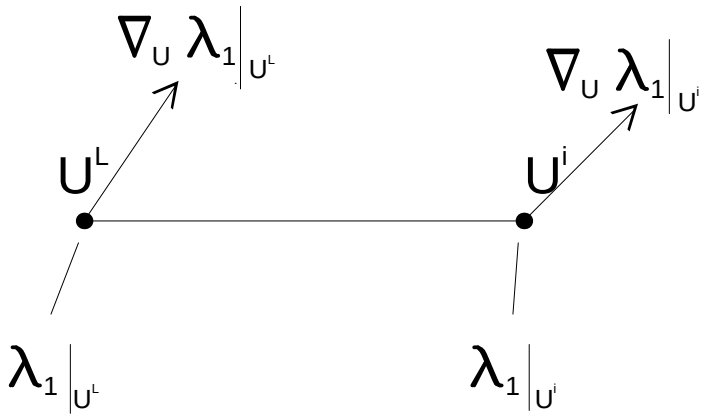

Figure 4.4: The parameters needed in the wavespeed approximation process on path $\overline{\Gamma}_1$

and provide the second derivative information that is needed to compute a cubic approximation of the wavespeed λ_k along $\overline{\Gamma}_k$. A cubic approximation is used so that inflexion points in the flux can be represented. An additional simplifying procedure can also be introduced by replacing the cubic by its piecewise linear approximation in order to avoid finding zeroes of a cubic in the algorithm. Hence we need to compute the extrema of the cubic and then the piecewise linear approximation $\overline{\lambda}_k$ is defined to be the piecewise linear interpolant of the wavespeed at the two ends of the path and the extremum states. We note that analytic expressions for the gradients of the wavespeeds in (4.2.10) may be difficult to obtain, as with the Black-Oil model. In this case an alternative approach may be used, described by Trangenstein [48], which amounts to sampling the wavespeeds at two interior points along the path $\overline{\Gamma}_k$ and then again forming a piecewise linear approximation.

We now turn to the possibility of encountering a point where strict hyperbolicity fails. In a neighbourhood of the eigenvector deficiency two of the eigenvectors become nearly parallel, which leads to large expansion coefficients in (4.2.7). The phase space approximation is not reasonable and its use with the flux computation (4.2.9) can introduce instabilities into the method. The test for eigenvector deficiency described in [2] uses the structural coefficients, for implementation with the Black-Oil model these are not available therefore the approximate tests described in [48] may be used. When we detect that two wavespeeds may coalesce,

say λ_l and λ_m, we only modify the treatment of the two wave families involved, the remaining families are treated as before. Hence we assume that $\overline{\mathbf{R}}_l$ and $\overline{\mathbf{R}}_m$ are nearly parallel and hence the associated expansion coefficients are unreliable. When more than two wavespeeds are involved the changes are a natural extension to the two-mode case.

The modifications needed depend on whether the eigenvector deficiency is associated with a change in sign of the wavespeed during the transition from $\mathbf{U}^L$ to $\mathbf{U}^R$. To test for this the following are defined

$$\lambda_{lm}^{min} = \min(\lambda_l^L, \lambda_l^R, \lambda_m^L, \lambda_m^R),$$

$$\lambda_{lm}^{max} = \max(\lambda_l^L, \lambda_l^R, \lambda_m^L, \lambda_m^R).$$

If λ_{lm}^{min} and λ_{lm}^{max} are of the same sign it is assumed the deficiency is not associated with a transonic wave. In this case the portion of the jump

$$\overline{\alpha}_l \overline{\mathbf{R}}_k + \overline{\alpha}_m \overline{\mathbf{R}}_m,$$

is collapsed into a single jump which is denoted by $\overline{\mathbf{R}}_{lm}$ and is of length $\overline{\alpha}_{lm}$. A modified flux is then defined, which in the case of the reference state being the left is

$$\mathbf{F}^{EO} = \mathbf{F}(\mathbf{U}^L) + \sum_{k \neq l,m} \left(\int_0^{\overline{\alpha}_k} \min(\overline{\lambda}_k, 0)\, d\alpha \right) \overline{\mathbf{R}}_k + \left(\int_0^{\overline{\alpha}_{lm}} \min(\overline{\lambda}_{lm}, 0)\, d\alpha \right) \overline{\mathbf{R}}_{lm},$$

where $\overline{\lambda}_{lm}$ is a linear function which satisfies

$$\overline{\lambda}_{lm}(0) = \max(\lambda_l^L, \lambda_m^L),$$

$$\overline{\lambda}_{lm}(\overline{\alpha}_{lm}) = \min(\lambda_l^R, \lambda_m^R).$$

When λ_{lm}^{min} and λ_{lm}^{max} are of opposite signs the integral correction terms are replaced by a dissipative term similar to that which is incorporated into Rusanov's scheme [37], the modified flux is then given by

$$\mathbf{F}^{EO} = \mathbf{F}(\mathbf{U}^L) + \sum_{k \neq l,m} \left(\int_0^{\overline{\alpha}_k} \min(\overline{\lambda}_k, 0)\, d\alpha \right) \overline{\mathbf{R}}_k - \frac{1}{2} \nu \overline{\alpha}_{lm} \overline{\mathbf{R}}_{lm},$$

where

$$\nu = \max(|\lambda_l^L|, |\lambda_m^L|, |\lambda_l^R|, |\lambda_m^R|).$$

The modified flux formulae for the cases when the reference state is the right state are easy to deduce by comparing with (4.2.9).

The ngquist-Osher flux is known to diminish the total variation of the solution to scalar conservation laws. However for the system case the approximate paths in state phase, between the left and right traced states, may not be a good representation of the true paths in state space. This is because at certain points the system may exhibit a lack of strict hyperbolicity and genuine nonlinearity. Therefore the calculated flux could possibly introduce some oscillation into the results. This is then damped out by addition of an artificial viscosity term which also ensures satisfaction of the entropy conditions and is described in the next subsection.

We need to ensure the numerical solution converges to the correct physical solution satisfying appropriate entropy conditions. This is ensured by the addition of a small amount of numerical diffusion. The amount of which must be carefully selected otherwise fronts may become excessively smeared. Therefore in the case of the second order scheme the flux in (4.2.9) is modified by addition of a

by Collela and Woodward [11] and is of the form

$$0\ 1\max(\qquad\qquad 0)(\qquad\qquad)$$

This is of $(\Delta\quad)$ and hence also maintains the accuracy of the method. Collela and Woodward [11], also used the parameter of 0 1. This parameter of 0 1 has been used successively with a number of Godunov type methods. Some schemes are reported in [11] to require more viscosity, and hence have a parameter greater than 0 1.

No artificial viscosity is added for the first order scheme as an ample amount of diffusion will already be present due to the discretisation. The numerical fluxes in (4.2.11) are then used in the conservative difference formula to update the cell averages.

$$= \qquad \frac{\Delta}{\Delta}(\quad \bar{\ } \qquad \bar{\ }) \qquad\qquad (4\ 2\ 12)$$

4.3 Extension to Higher Dimensions

In multi-dimensions a central concern is the choice of the unsplit versus split methodology, which can have an effect on the overall computational efficiency of the scheme. An operator split algorithm would involve applying 1-dimensional operators in their particular coordinate direction separately, in order to advance the solution to the next time level. There being a rule by which the separate advancements of the solution in each coordinate direction are combined to achieve

to consider an unsplit scheme, and again follow the work of Collela [10] when describing a multi-dimensional Higher Order Godunov method. We restrict ourselves here to the 2-Dimensional scheme since higher dimensional schemes follow on naturally from this description.

We note that an alternative form of an unsplit multidimensional Higher Order Godunov method has been developed by Bell, Dawson and Shubin [3]. In this formulation a limited piecewise bilinear approximation of the solution in each grid cell is used to ensure oscillation free results. The left and right states at the cell edges being traced using the geometry of the characteristic surfaces. However this method has only been applied to scalar conservation laws, the authors of [3] stating that extension to systems of conservation laws would be difficult; we do not consider this method any further.

Firstly we state that we are considering the following 2-Dimensional systems of hyperbolic conservation laws

$$\frac{\partial}{\partial} + \frac{\partial}{\partial} + \frac{\partial}{\partial} = 0$$

where $=$ $($ $)$ and with initial data

$$(\quad 0) = \quad (\quad)$$

The numerical solution procedure largely proceeds as in the 1-Dimensional case. We calculate left and right traced states at each cell edge and hence solve the Riemann problems there. The jump between these two states is assumed to take place perpendicular to the cell edge, hence we solve 1-Dimensional Riemann problems at all the cell edges. The resulting fluxes, which are calculated in both

the state

since the other left states are calculated by interchanging the roles of and , and , and the right (R) states follows on naturally from our experience of the 1-D algorithm. We proceed as in the 1-D algorithm and use a Taylor's series extrapolation to the half time level and the cell edge in the coordinate direction. We again use the quasi-linear form, with respect to the direction, of the hyperbolic equations i.e. we use

$$\text{—} + \quad \text{—} + \text{—} = 0$$

to replace the temporal derivative of in the formula for , where is the -directional Jacobian —. We therefore have

$$= \quad + \frac{1}{2}(\Delta \quad \Delta \quad)\text{—} \quad \frac{\Delta}{2}\text{—}$$

which looks like the 1-D traced states with an extra term due to the extra coordinate direction, i.e. the fact that we are working in two dimensions. We again apply the characteristic projection operators to the second order tracing terms, they are neglected here to simplify the exposition.

The tracing of this left state can be viewed as a 2 step procedure by firstly calculating the traced states as in the 1-D case by replacing — with its monotonised central difference approximation, i.e.

$$= \quad + \frac{1}{2}(\quad \frac{\Delta}{\Delta} \quad)\Delta$$

Secondly we add on the effect of the transverse flux gradient —, i.e.

$$= \quad \quad \frac{\Delta}{2}\text{—} \qquad (4\ 3\ 13)$$

—

—

where

$$(\qquad)$$

denotes the flux obtained from solving the Riemann problem with the indicated left and right states. So Godunov's first order method used to approximate — would take

$$\_ =$$

$$\_ = \tag{4 3 14}$$

i.e. the cell centred quantities.

However for problems involving moderately strong discontinuities traveling obliquely to the grid directions, it is necessary to use a more accurate approximation to the transverse derivative. This is because if the approximation calculated is sufficiently different from the actual change calculated in the conservation (conservative update) step then the solution will overshoot or the discontinuity will spread. To address this possible problem more accurate left and right states

1. Compute 1-D left and right traced states at each cell interface in each coordinate direction,
2. Add on the effect of the transverse flux derivatives to all the traced states,
3. Solve 1-D Riemann problems at every cell interface,
4. Use a conservative difference formula to update the cell averages,

$$\mathbf{U}_{i,j}^{n+1} = \mathbf{U}_{i,j}^{n} - \frac{\Delta t}{\Delta x}(\mathbf{F}_{i+\frac{1}{2},j}^{n+\frac{1}{2}} - \mathbf{F}_{i-\frac{1}{2},j}^{n+\frac{1}{2}}) - \frac{\Delta t}{\Delta y}(\mathbf{G}_{i,j+\frac{1}{2}}^{n+\frac{1}{2}} - \mathbf{G}_{i,j-\frac{1}{2}}^{n+\frac{1}{2}}).$$

In the next chapter we describe the implementation of the Higher Order Godunov scheme on the Black-Oil model, and show results of numerical reservoir simulations in 1 and 2 dimensions.

Chapter 5

Implementation of the Higher Order Godunov Method on the Black-Oil Flow Equations

5.1 Introduction

In this chapter we discuss the implementation of the Higher Order Godunov method on the Black-Oil fluid flow equations. We also describe the general computational details associated with the numerical modelling, such as time step control and the type of computational grid used, and also discuss the discretisation of the parabolic pressure equation. A 1-D and a dimensionally unsplit 2-D Fortran code were written to numerically solve the flow equations so we may perform reservoir simulations in 1 and 2 dimensions. The 1-D code was validated by comparison of results with those presented by Trangenstein and Bell in [46], who also applied the Higher Order Godunov method to the Black-Oil equations. We show results of three of these comparison problems.

Results of a 2-D cross-sectional problem, using the same numerical method and mathematical model, are shown by Bell et al. in [2] but the initial conditions are not supplied therein. No other 2-D Black-Oil results have appeared in the literature, so the 2-D code was validated by comparison of results with those from a commercial reservoir simulator. These comparisons relate more closely to the discussions in Chapter 7 and can be found there. However, in this chapter we

present results of a 2-D Areal problem which was used to investigate the effect on the numerical results of the accuracy of the transverse flux derivatives (4.3.15) and (4.3.14), described in Section 4.3.2.

It is not possible to construct analytic solutions to the Black-Oil fluid flow equations but analytic solutions to 3-phase incompressible flow equations are possible. Comparison of the analytic solutions of these problems with the corresponding numerical results has not appeared in the literature. Incompressible flow problems are a good test of a numerical method since analytic solutions exist for comparison with numerical results. Construction of analytic solutions in this case is straightforward since the mathematical model for incompressible flow reduces to a 2-system of conservation laws. The model also exhibits local linear degeneracies and eigenvector deficiencies, as does the Black-Oil model, and hence is a good test of the numerical method, although for the types of problem considered, namely those with no gravitational effects and therefore no counter-current flow, the Higher Order Godunov scheme used to simulate the problems is not fully tested. This is because the phase space construction of the Riemann problem described in Section 4.2.3, will not be needed because the flux computation reduces to upwind determination. Physical assumptions and experience of incompressible flow problems are used to aid the solution construction process. The Higher Order Godunov method was found to be successful at simulating these incompressible (Buckley-Leverett) flow problems and so confidence is provided that the numerical method is resolving the solutions to the analogous Black-Oil model problems well. Some numerical results of 3-phase incompressible flow problems were also presented by Bell et al. [6] but these were not compared against analytic solutions since they were used to investigate the prescence of elliptic degeneracies in the conservation laws.

Finally in this chapter we describe the incorporation of source terms to model injection of fluid into and production of fluid from the reservoir. Source terms are traditionally used in the computer codes used by the reservoir simulation community to model these processes. However as far as we know source terms have not previously been used in conjunction with the form of the Black-Oil model in [46] but have been used with the much simpler Polymer Flood Model

[49], neither of these models being used in commercial reservoir simulation codes. Locally implicit procedures are usually utilised when applying source terms to remove the numerical stability problem associated with their use. We follow this approach when applying source terms in conjunction with the Black-Oil model and Higher Order Godunov method.

5.2 omputational Approach

5.2.1 Computational Grids

The discretisations of the differential equations are based on a block (or cell) centred grid system. The block centred grid is particularly suitable for reservoir simulation problems because fluid and rock properties can be assigned, and assumed to hold throughout each computational cell. The 1-Dimensional grid is specified by giving the grid block interfaces which are denoted by

$$\cdots x_{j-\frac{1}{2}} < x_{j+\frac{1}{2}} < \cdots,$$

with an analogous definition of the grid in higher dimensions. The block centred grid can be distinguished from the more standard point (or node) centred grid in the following way. The block centred grid can be considered as the computational region having been distributed with cells, with the nodes residing in their centres, whereas the node centred grid having been distributed with nodes. Therefore the two ends of the block centred grid align with block edges, whereas in the case of the point centred grid the ends of the grid align with nodes and hence a half cell is present at the ends of the grid. Again in two dimensions all the boundaries of the grid, assuming it is regular, align with block edges. In 1-Dimension grid block B_j is bounded by $x_{j-\frac{1}{2}}$ and $x_{j+\frac{1}{2}}$ and is of length $\Delta x = x_{j+\frac{1}{2}} - x_{j-\frac{1}{2}}$.

For each grid block B_j we define a vector of component densities at time t which is denoted by $\mathbf{n}_j^n$, and provides a piecewise constant approximation to $\mathbf{n}$ at time t. A pressure p_j^n is associated with each $\mathbf{n}_j^n$ and at time $t = 0$, i.e. the initial conditions, p and $\mathbf{n}$ should be paired such that the volume balance equation (3.4.4) is satisfied. A staggered grid is used with pressure and component densities stored at grid block centres and with total velocities stored at grid block interfaces, see

Figure 5.1. This is due to the centred discretisation of Darcy's law (5.2.2) and is standard in reservoir simulation work, see Aziz and Settari [1].

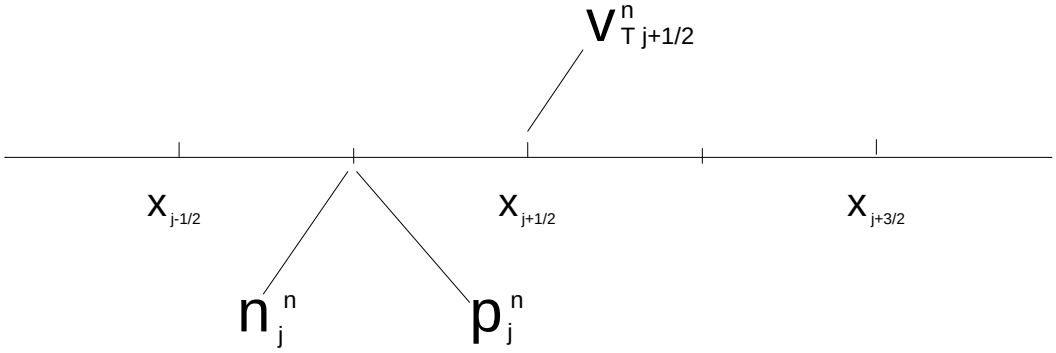

Figure 5.1: The staggered 1-D grid, indicating where the variables pressure ( ), component density ( ) and total velocity ( ) are stored.

The use of a block centred grid with the Higher Order Godunov method is also particularly suitable due to the cell based nature of the scheme. Also specification of numerical boundary conditions is straightforward. For example at $= 0$ we have the first cell edge where we need to specify a flux, so if we have an inflow boundary we assign the physical inflow flux there. On the other hand if the boundary is of no-flow type then we simply set the flux to zero. At the other end of the 1-D grid, at $=$ say, we also need to specify a flux. The no-flow boundary is treated as before, but if we have an outflow boundary then we can perform a characteristic tracing of to the boundary, as in the internal flowfield, and calculate the resulting outflow flux.

The system of conservation laws (3.5.8) is discretised using the Higher Order Godunov method described in the previous chapter. There are a number of points regarding implementation with the Black-Oil model worth mentioning. Firstly, due to the high component density of gas, because of its high compressibility, the component densities are poorly scaled. This results in an unreliable calculation of the average wavespeed (4.2.8), used to determine the reference state for the flux computation. This can be overcome, see [49], by multiplication of and

As the numerical solution of the pressure equation is of implicit type there is no restriction on the time step due to stability considerations. The solution of (5.2.1) after substitution of (5.2.2) is accomplished by solving a tridiagonal linear system every time step. This system is straightforward to solve directly via a standard forward/backward substitution algorithm, and in any case is the most efficient, see Golub and van Loan [21].

We note however, that the fluid parameters in the discretisations (5.2.1) and (5.2.2) can only be evaluated at the current time level, because they are functions of the quantities we are trying to calculate. This results in the approximation of pressure being second order accurate in space but only first order in time. The fact that pressure is only first order accurate in time is not thought to be too serious by Trangenstein [49]. This is because although pressure effects are quickly felt throughout the reservoir, once the fluid flow has settled down the pressure field is slowly varying in time because of the small compressibilities in the reservoir fluids, i.e. the coefficient of — is of the order 10 . Therefore the time truncation errors associated with the pressure equation should not be too large compared to those in the hyperbolic conservation laws.

The transmissibilities _ in (5.2.1) and (5.2.2), at the cell interfaces are formed by a harmonic weighting

$$_{-} = \frac{2}{+}$$

the other quantities at the cell interfaces being evaluated by arithmetic averaging, for example

$$_{-} = \frac{1}{2}(\quad + \quad)$$

The reason for the differing methods of calculation of the quantities needed at

transmissibilities τ. This is because he is very keen to stress the equivalence of the discretisation, along with the given method of obtaining the cell edge coefficients, with the mixed finite element formulation of the pressure equation. If all the coefficients were harmonically averaged, as the above reason dictates, this would not then be the case.

5.2.3 Time Step Control

Time step control for the component conservation equations is based on CFL [13] considerations,

$$\Delta t^n \leq \frac{\Delta x}{S^n_{max}},$$

where S^n_{max} is the largest wavespeed at the current time level. As we are approximating the solution of the differential equations with the numerical method, the possibility exists that the maximum wavespeed calculated S^n_{max} could be smaller than the maximum wavespeed in the analytic solution. This would result in the calculated time step being an unstable one. To allow for this possibility the calculated time step is reduced by a multiplicative factor termed a CFL number. A CFL number of 0.9 is usually sufficient for use with the Higher Order Godunov method, to achieve stable numerical solutions.

This time step is also suitable for correctly capturing the transient behaviour in the parabolic pressure equation. To justify this we can examine how the time step responds to fluctuations in the pressure field. The time step is inversely proportional to the wavespeed which is proportional to the total velocity v_T, i.e.

$$\Delta t \propto \frac{\Delta x}{S_{max}} \propto \frac{\Delta x}{v_T},$$

and since in the absence of gravitational effects $v_T \propto \frac{\Delta p}{\Delta x}$, we have

$$\Delta t \propto \frac{(\Delta x)^2}{\Delta p}. \tag{5.2.3}$$

Time steps of $O(\Delta x^2)$ are of the correct size for ensuring stability in explicit numerical solutions of parabolic equations, however, we are using an implicit discretisation which has a far less severe stability criteria, if indeed any. The relation (5.2.3) tries to ensure that the $O(\Delta t)$ and $O(\Delta x^2)$ leading terms in the truncation error balance.

When we solve the pressure equation we use a time step based on CFL considerations at the current time level. Once the pressure field at the advanced time level is obtained we may calculate the maximum wavespeed and hence an associated stable time step at this level. If this time step is greater than that at the current time level we complete the update procedure by solving the conservation laws, if this is not the case we repeat the pressure equation with the stable time step from the advanced time level. Thus this process represents an extra technique of ensuring stability and is important in problems with high injection rates. This strategy of ensuring a stable time step can be summarised by

$$\Delta \qquad \frac{\Delta}{\max\ (\quad (\quad)\quad (\quad))}$$

The time stepping used in the Higher Order Godunov code is based on CFL criteria with a CFL number of 0.9. However we need to supply the code with an initial time step since at $= 0$ all wavespeeds are zero. We supply a very small time step of 0.001 days to break the computation in. Also we do not allow the increase of the time step to go beyond a specified limit, an increase of a factor of 1.5-2.0 is usually acceptable which has the effect of controlling the volume error discrepancy which can become large near the wells early on, due to the comparatively large changes in pressure and component density there. Once the computations have settled down the usual CFL criteria then takes over in controlling the time steps. Also, during the course of the computation, if large v iffxCx[s(NpxC([iffsffxC34N(N5ffx4N3fffixC3v

up a considerable amount of the total CPU time, i.e. around 20 . Therefore we require the method of solution to be as efficient as possible so we prefer an iterative method such as the Successive Line Over Relaxation (SLOR) method, see Varga [52] for details, or the pre-conditioned Conjugate Gradient method see Golub and van Loan [21] for general details and Van Der Vorst [53] for the algorithm used. We tried both methods of solution and found the pre-conditioned conjugate gradient method to be more efficient as the grid was refined.

We now describe the implementation of boundary conditions for a 2-D Areal reservoir simulation problem. An Areal problem takes place in the $x - y$ plane, gravity is assumed to act in the z-direction, therefore there are no gravitational effects in the problem, if there is no dip angle in either coordinate direction. See Aziz and Settari [1] for a more detailed description of the Areal problem and for other types of reservoir simulation performed in 2-D, for example cross-sectional problems which do include gravitational effects. The Areal region is usually square with injection of fluid taking place in the bottom left hand corner and production of fluid in the top right hand corner. All boundaries other than the injection and production points are of no normal flow type. The computational region is shown in Figure 5.3.

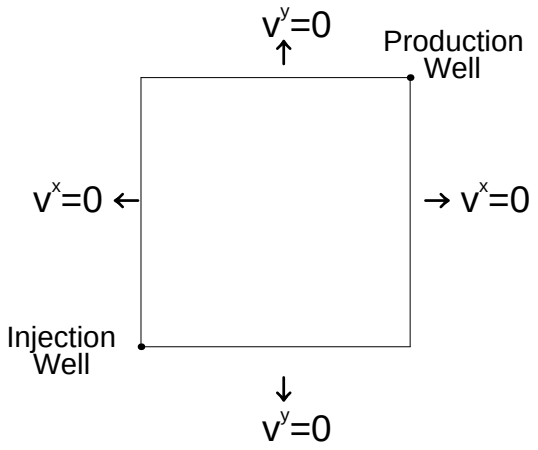

Figure 5.3: The geometry of the Areal problem, indicating the locations of the wells and the no-flow boundaries.

The grid block in the bottom left hand corner containing the injection well is shown in Figure 5.4.

We need to specify the four fluxes shown on Figure 5.4 to update the compo-

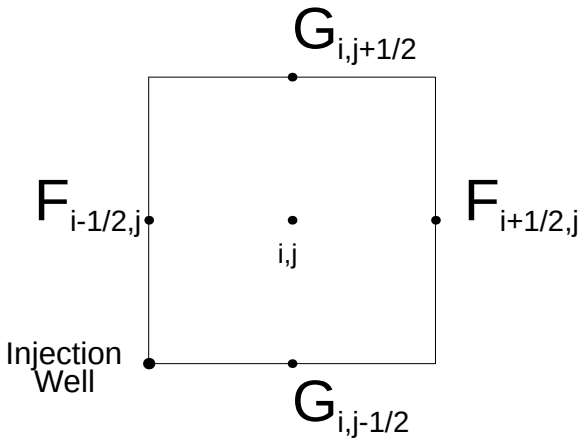

Figure 5.4: The injection grid block, indicating the 4 fluxes needed to update the component density vector.

nent density held at the block . The two fluxes _ _ are calculated using the methods explained in Chapter 4. We see that the fluxes _ _

_ _ _ _

_ _

conservative finite difference update, the same process as in the 1-D case. Again this modelling of production is also used in the pressure equation.

5.3 Validation of the Higher Order Godunov ode

A Fortran code was written to solve the Black-Oil fluid flow equations given in Chapter 3 using the Higher Order Godunov method described in Chapter 4. Both a 1-D and a dimensionally unsplit t5[BotLLC([co4NxfiCx[dIit4Nx3w[giv4xfiCx[rdIit4Nx3wC3

water. The initial fluid distribution was taken to be uniform along the length of the reservoir, and had an associated pressure. Fluid of given composition and pressure was injected at $= 0$ and the fluid resident in the reservoir was produced at a specified pressure at $= 1000$. We remark that the initial data, of the problems given in [46], including that at injection and production did contain a volume error discrepancy, i.e. the volume balance equation (3.4.4) was not satisfied exactly.

The problems were simulated using the second order scheme with 200 grid blocks to accurately resolve the fronts, a CFL number of 0.9 was used throughout

problem A3, and has injection and initial reservoir compositions given by,

$$= \begin{matrix} 0\ 404 \\ 4\ 042 \\ 0\ 647 \end{matrix} \qquad = \begin{matrix} 0\ 734 \\ 32\ 10 \\ 0\ 1835 \end{matrix}$$

This problem is an undersaturated flow example with the vapour phase missing. The injection, initial reservoir and production pressures are 1400, 1200 and 1000 psi respectively. The simulation time being 300 days with the results from the Higher Order Godunov code shown in Figure 5.7. The corresponding results shown by Trangenstein and Bell in [46] are shown in Figure 5.8.

Both wavespeeds in the saturated flow problem 1 are termed Buckley-Leverett modes, due to their similarity to the 3-phase incompressible wavespeeds. In undersaturated flow only one of the wavespeeds is of this form, the other being the linearly degenerate particle velocity. Hence only one of the two wave modes was expected to yield a compound wave similar to those observed in problem 1. The compound wave in Figure 5.7 can be identified, with the shock located around 750 feet.

The last 1-D example is problem 5 from [46], which we refer to as problem A4, and has injection and initial reservoir compositions given by,

$$= \begin{matrix} 0\ 0179 \end{matrix}$$

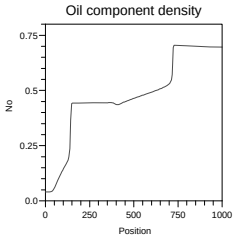
Oil component density
No
0.75
0.5
0.25
0.0
0
250
500
750
1000
Position

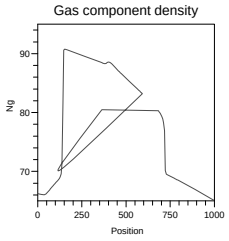
Gas component density
Ng
90
80
70
0
250
500
750
1000
Position

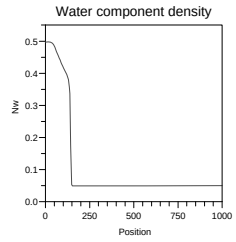
Water component density
Nw
0.5
0.4
0.3
0.2
0.1
0.0
0
250
500
750
1000
Position

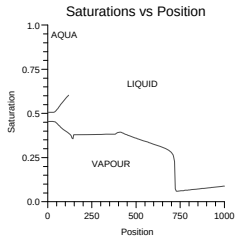
Saturations vs Position
Saturation
1.0
0.75
0.5
0.25
0.0
AQUA
LIQUID
VAPOUR
0
250
500
750
1000
Position

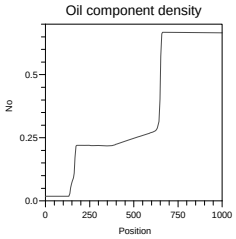
Oil component density
No
0.5
0.25
0.0
0
250
500
750
1000
Position

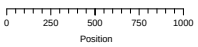
0
250
500
750
1000
Position

accuracy of the these terms is expected to be more noticeable since transverse flow is more prevalent.

xperience of Black-Oil computations have provided a feel for the level of volume error discrepancy that is acceptable in terms of the accuracy of the numerical results. For instance in 1-D computations without gravity the maximum volume error discrepancies generated are typically in the range (10) (10) which are deemed acceptable. If discrepancies of (10) are generated these are thought to be unacceptable and may usually be reduced by reducing the time step. For example when fluid is injected having an associated volume error discrepancy of (10) boundary layers develop in the results at the injection point. This is due to the mismatch in discrepancy between the injected fluid and the fluid in the reservoir, and represents unphysical behaviour. In 2-Dimensional simulations the volume error discrepancies generated are typically an order of magnitude higher than those in 1-D.

5.4 onstruction of Analytic 3-Phase Flow Riemann Problem Solutions

We now move on to the construction of analytic solutions to the Riemann problem associated with 3-phase incompressible flow equations in order to test the accuracy of the Higher Order Godunov method when applied to degenerate systems of conservation laws. Analytic Riemann problem solutions for 3-phase compressible flow problems do not exist due to the complexity of the mathematical model. However analytic Riemann problem solutions for 3-phase incompressible problems without gravitational effects are relatively straightforward to construct. We construct some 3-phase incompressible analytic solutions and compare these with the corresponding results from the Higher Order Godunov code. Some ana-

ing to a 2-system of equations due to the volume balance condition. The mass conservation equations for the 3 fluid components (or phases) are as follows

$$\frac{\partial}{\partial t}(n_i\phi) + \frac{\partial}{\partial x}(\rho_i v_i) = 0,$$

where $i = o, g, w$ and refers to the fluid component with component density n_i. ϕ is the porosity, ρ_i is the density of the phase and v_i is the gravity free Darcy phase velocity given by

$$v_i = \frac{\lambda_i v_T}{\lambda_o + \lambda_g + \lambda_w},$$

where λ_i are the phase mobilities and v_T is the total fluid velocity. No mass transfer effects are modelled and so the phases and components are equivalent. For example oil exists in the liquid phase only and so the liquid phase could equally well be referred to as the oil phase, similarly for gas and water. The following equations describe phase equilibrium

$$n_i = \rho_i s_i, \quad i = o, g, w,$$

where s_i is the phase saturation which is the volume fraction of the phase. Hence the saturations sum to one, which gives the volume balance equation

$$s_o + s_g + s_w = 1. \tag{5.4.5}$$

The conservation of mass equations may be manipulated to give

$$\phi\frac{\partial \mathbf{s}}{\partial t} + \frac{\partial \mathbf{v}}{\partial x} = 0,$$

where $\mathbf{s}$ and $\mathbf{v}$ are vectors of the component quantities. These 3 equations may be summed to give the relation

$$\frac{\partial v_T}{\partial x} = 0,$$

which states that the total fluid velocity is independent of position in the reservoir. This means that the boundary conditions specify the velocity field throughout the reservoir. Only 2 of the saturation equations need to be considered, namely

$$\frac{\partial s_w}{\partial t} + \frac{\partial v_w}{\partial x} = 0,$$

and

$$\frac{\partial s_g}{\partial t} + \frac{\partial v_g}{\partial x} = 0,$$

since (5.4.5) then implies conservation of the oil saturation s_o. Hence we have a conserved variable $\mathbf{U} = [s_w, s_g]^T$ of saturations and a flux function vector $\mathbf{F} = [v_w, v_g]^T$ of phase velocities.

The characteristic structure of the model is as follows, the wavespeeds are given by

$$\lambda_{1,2} = \frac{1}{2}\left[\frac{\partial v_w}{\partial s_w} + \frac{\partial v_g}{\partial s_g} \mp \sqrt{\left((\frac{\partial v_w}{\partial s_w} - \frac{\partial v_g}{\partial s_g}) + 4\frac{\partial v_g}{\partial s_w}\frac{\partial v_w}{\partial s_g}\right)}\right],$$

and the right eigenvectors by

$$\mathbf{r}_1 = \begin{bmatrix} 1 \\ \frac{\lambda_1 - \frac{\partial v_w}{\partial s_w}}{\frac{\partial v_w}{\partial s_g}} \end{bmatrix}, \mathbf{r}_2 = \begin{bmatrix} 1 \\ \frac{\lambda_2 - \frac{\partial v_w}{\partial s_w}}{\frac{\partial v_w}{\partial s_g}} \end{bmatrix}.$$

It is known that the wavemodes of this model are not genuinely non-linear. Therefore shock/rarefaction compound waves which also occur in the 2-phase Buckley-Leverett model will be expected.

Weak solutions of the flow equations are sought as discontinuous solutions are expected. The Riemann problem considered is of the form

$$\mathbf{s}(x,0) = \begin{cases} \mathbf{s}^L & \text{if } x = 0 \\ \mathbf{s}^R & \text{if } x > 0 \end{cases},$$

so that s^L corresponds to the injected fluid composition and s^R the initial reservoir composition. The theory of the Riemann problem solution to a 2-system of strictly hyperbolic conservation laws can be found in Smoller [41]. Liu [30] describes the solution of the Riemann problem for systems not satisfying the genuine non-linearity condition.

The calculated analytic solutions are plotted against the wavespeed x/t which leads to a clearer interpretation of the results. Some analytic results will be shown after a description of the construction process and compared to numerical results from the Higher Order Godunov code. We use the same relative permeability functions as were used with the Black-Oil computations, given in Section 3.9, and the following phase viscosities in Centipoise

$$\mu_o = 1.0, \quad \mu_g = 0.05, \quad \mu_w = 0.8.$$

is successively applied to the injected water saturation, which defines the left state of the rarefaction. The wavespeed is calculated and plotted against since for a 1-rarefaction we have = . The incrementation procedure on the water saturation which constructs the 1-rarefaction is continued until the location of the shock which connects the current water saturation on the rarefaction wave to the initial reservoir water saturation is found. The 1-shock is located as follows; since the shock is part of a compound wave connected to a 1-rarefaction then at the connection point, say, the 1-rarefaction is given by

$$- = \quad (\quad)$$

the 1-shock is located at = , where is the shock speed and hence the shock will have speed

$$= \quad (\quad)$$

which satisfies the extended entropy condition for shocks which aaix[t4N(xffCS[the4N(ffCS[,4ffPfi)(

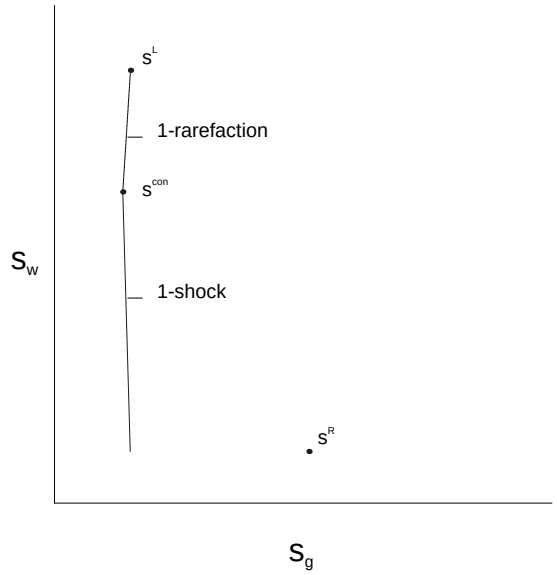

Figure 5.14: xample wave curves in phase space emanating from the left state in the Riemann problem.

where is the shock speed and the superscripts indicate the left and right states associated with the shock. The only unknown in this non-linear equation is since the oil saturation to the right of the shock may be expressed in terms of and , and may be calculated by using an iterative method such as Newton. Now the characterisation of the shock can be checked to see if it satisfies the appropriate entropy condition, namely that it is a 1-shock. Assuming this to be the case, we can now attempt to connect the local right state associated with the 1-shock to the right state in the Riemann problem, i.e. the initial reservoir conditions, by a 2-wave. A triple (transitional) wave is not considered a possibility, as these are not typically seen in gravity free 3-phase flow problems, and would only occur at an umbilic point, so a constant state connects the local right state to the 2-wave.

The wavespeeds associated with the local right state and the reservoir initial

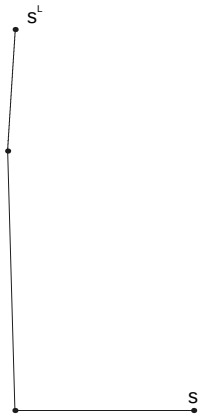
S^L
S

be connected from to the initial reservoir state. This is done by calculating the shock speed

$$= \frac{\qquad}{\qquad}$$

and then using this in the entropy condition

which is of the required form for determining the admissibility of a shock in a rarefaction-shock compound wave. If this condition is satisfied then we have found the 2-shock in the compound wave located at = . This then completes

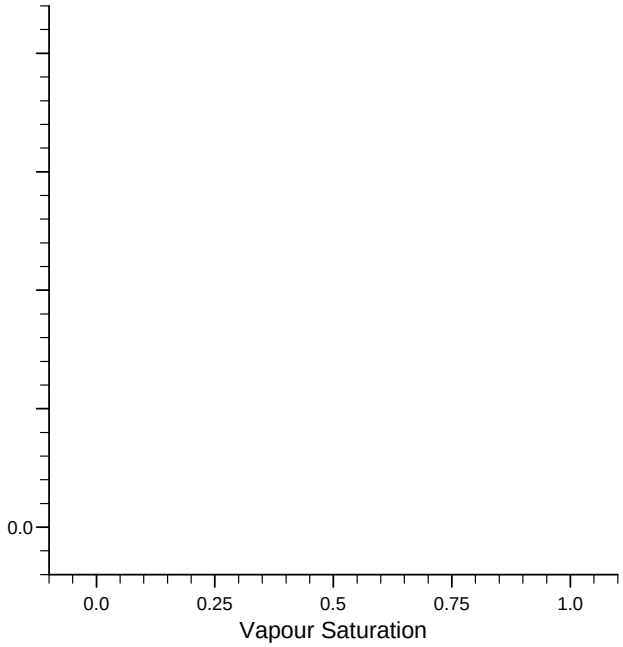
0.0
0.0
0.25
0.5
0.75
1.0
Vapour Saturation

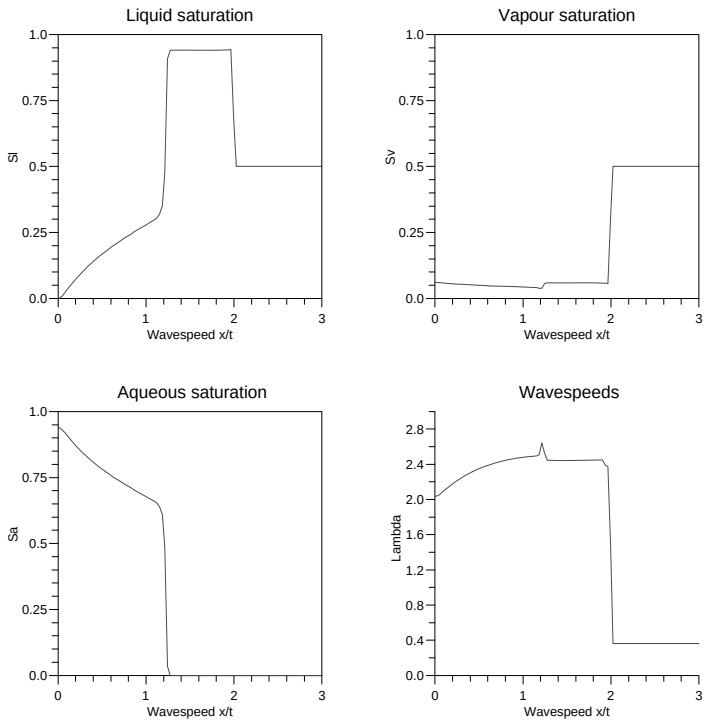
Liquid saturation
Sl
Wavespeed x/t
Vapour saturation
Sv
Wavespeed x/t
Aqueous saturation
Sa
Wavespeed x/t
Wavespeeds
Lambda
Wavespeed x/t

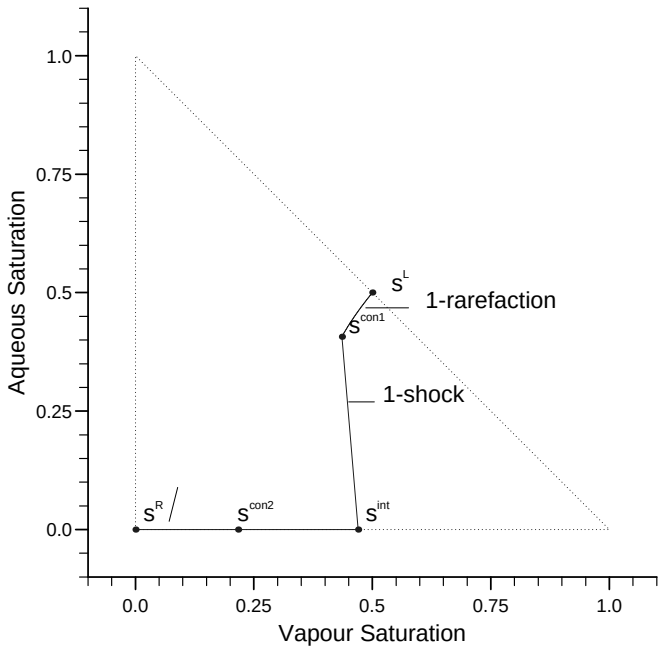
1.0
0.75
0.5
0.25
0.0
Aqueous Saturation
0.0
0.25
0.5
0.75
1.0
Vapour Saturation
S^L
1-rarefaction
S^con1
1-shock
S^R
S^con2
S^int

The 2-rarefaction is tracked until a valid 2-shock can be found which connects the rarefaction to the initial reservoir state. A 2-shock with speed $= 2\,791$ was found to accomplish this. The corresponding numerical results, again run with 100 grid blocks, are shown in Figure 5.21. The analytic solution contains some fine detail in the vapour saturation profile, the 1-rarefaction-shock poses

5.5 Incorporation of Source Terms

pressure equation now becomes

$$c\frac{\partial p}{\partial t} + \quad ^{T}\frac{\partial}{\partial x}(\ v_T + \quad \tau) = q + \quad ^{T}RB \quad .$$

The additional source term here represents no problem in its numerical solution. However this is not the case when we come to solve the conservation laws as previously described. If we wish to model injection of fluid into the reservoir, then the source term will only appear in the equations associated with that grid block. Hence the implicit procedure to be described need only be used when variables associated with that grid block are used in the calculations.

The locally implicit procedure for a source in block j as outlined by Holing et al. [26] is as follows. The cell edge fluxes $_{j\ -}$ and $_{j\ -}$ are calculated as the first order upstream implicit fluxes. Therefore for flux $_{j\ -}$ this means that if the fluid flow is into this cell edge from right to left then the flux calculation is explicit. If the flow is from left to right then the well cell variables will be needed to calculate the flux and hence the implicit procedure is needed. For example the implicit procedure for a constant source in cell j with flow from left to right would be

$$(\ \phi)_j^n\ ^{-} = (\ \phi)_j^n - \frac{\Delta t}{2\Delta x}\quad (\ _j^n\ ^{-}, p_j^n\ _{-}^{-}, (v\ )\ _{-}^{-}) - \quad _{-}^{-} + \frac{\Delta t}{2}\quad , \qquad (5.5.6)$$

where is the source term. The flux $_{-}^{-}$ is calculated to second order, explicitly in the usual manner as the well cell is not upstream for this flux calculation. quation (5.5.6) is implicit in $^{-}$ and so we need to solve it by an iterative method. Hence the main idea behind the procedure is calculation of an implicit well cell flux rather than an implicit update of the component density in the well cell. Once the unknown $^{-}$ has been calculated the flux $_{-}^{-}$ may be recalculated explicitly using $^{-}$ and used in the usual finite difference update procedure, which will also include the source term, i.e.

$$(\ \phi)\quad = (\ \phi)\ - \frac{\Delta t}{\Delta x}\quad _{-}^{-} - \quad _{-}^{-} + \Delta t \quad .$$

The modelling of injection and production of fluid in a 1-D reservoir simulation was tried using point source terms. Firstly injection of fluid will take place via a source term in the centre of grid block 1 and hence the flux $_{-}$ (with $j = 1$) in

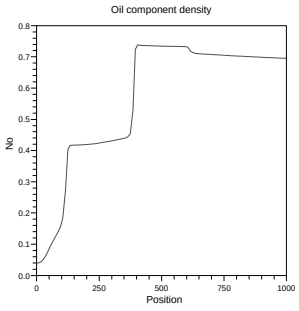
Oil component density
No
Position
0.0
0.1
0.2
0.3
0.4
0.5
0.6
0.7
0.8
0
250
500
750
1000

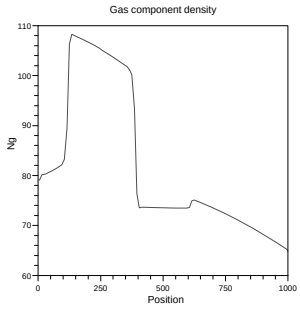
Gas component density
Ng
Position
60
70
80
90
100
110
0
250
500
750
1000

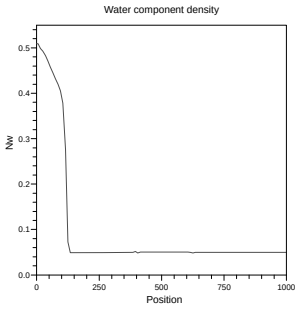
Water component density
Nw
Position
0.0
0.1
0.2
0.3
0.4
0.5
0
250
500
750
1000

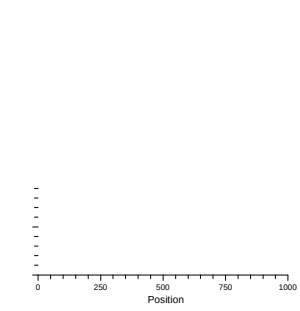
Position
0
250
500
750
1000

used is smooth, an improvement on the results from the explicit case. The results consist of two rarefaction-shock compound waves connecting to a constant state at about 400 feet. The region from 400 to 600 feet is an undersaturated region, hence the discontinuity in the slower wavespeed at these distances. This problem cannot be simulated using boundary fluxes rather than source terms, for comparison of results purposes, since both the pressure of the injected fluid and its injection rate may not simultaneously be specified.

In using the explicit second order flux calculation it should be noted that the source term in the conservation laws will appear in the characteristic tracing step of the Higher Order Godunov procedure. This is because the quasi-linear form of the conservation laws are used in that step of the computation. When we perform the characteristic tracing step we neglect the source term from that step since its inclusion causes unphysical solution behaviour. This can be justified since the presence of the source term causes the characteristics to be modified so instead of deriving these modified characteristics we simply neglect the source term.

We now discuss the modelling of a production source to model production of fluid from a production well. The source term will be located in cell Nx where Nx is the total number of grid blocks used in the simulation. The composition of the fluid being produced is the composition of the fluid that resides in cell Nx. The implicit flux calculation is of the form

$$(\mathbf{n}\phi)_{Nx}^{n+\frac{1}{2}} = (\mathbf{n}\phi)_{Nx}^{n} - \frac{\Delta t}{2\Delta x}\left[\mathbf{h}_{Nx+\frac{1}{2}}^{n+\frac{1}{2}} - \mathbf{h}_{Nx-\frac{1}{2}}^{n+\frac{1}{2}}\right] + \frac{\Delta t}{2}\mathbf{s}_{prod}^{n},$$

where $\mathbf{s}_{prod}^{n}$ is the source term representing the production fluid. The flux $\mathbf{h}_{Nx+\frac{1}{2}}^{n+\frac{1}{2}}$ is zero since the boundary at $x = x_{max}$ is of no-flow type. The flux $\mathbf{h}_{Nx-\frac{1}{2}}^{n+\frac{1}{2}}$ may be calculated explicitly to second order accuracy since the production source is not upstream with respect to the cell interface $Nx-\frac{1}{2}$. Hence the resulting equation is not implicit in $\mathbf{n}_{Nx}^{n+\frac{1}{2}}$ and hence need not be solved since the normal explicit update may be used instead, i.e.

$$(\mathbf{n}\phi)_{Nx}^{n+1} = (\mathbf{n}\phi)_{Nx}^{n} - \frac{\Delta t}{\Delta x}\left[-\mathbf{h}_{Nx-\frac{1}{2}}^{n+\frac{1}{2}}\right] + \Delta t\ \mathbf{s}_{prod}^{n}.$$

A totally implicit update of $\mathbf{n}_{j}^{n+1}$, using a first order implicit upstream flux $\mathbf{h}_{j+\frac{1}{2}}^{n+1}$, was also tried instead of the implicit flux calculation of $\mathbf{h}_{j+\frac{1}{2}}^{n+\frac{1}{2}}$. The implicit

update for a source in cell is then of the form

$$(\quad) \quad = (\quad) \quad \frac{\Delta}{\Delta} \quad (\qquad \_ (\quad) \quad \_) \qquad \bar{\_} + \Delta \qquad (5\ 5\ 7)$$

where the source term is upstream with respect to cell edge + - so that (5.5.7) is implicit in . However this procedure was not effective at modelling source terms since the iteration, of simple type, used to solve (5.5.7) would not converge.

The implicit flux calculation was also used to model a source term in the Areal 2-D problem. In this problem injection of fluid takes place in the lower left hand grid block and production of fluid in the upper right hand grid block. Also there are no gravitational effects in the problem. The production source may be incorporated explicitly as the well cell is not upstream for the relevant flux computations, similarly to the 1-D case. The injection source is located in grid block 1,1. The implicit flux calculation to model the source is as follows

$$(\quad) \quad \bar{} = (\quad) \qquad \frac{\Delta}{2\Delta} \quad (\quad \bar{} \quad \_ \bar{} \ (\quad)\_ \bar{})$$

$$\frac{\Delta}{2\Delta} \quad (\quad \bar{} \quad \_ \bar{} \ (\quad) \ \_ \bar{}) \ + \frac{\Delta}{2} \qquad (5\ 5\ 8)$$

The fluxes $\_$ and $\_$ are both zero as they lie on no-flow boundaries. The

$\_$ $\_$

$\_$

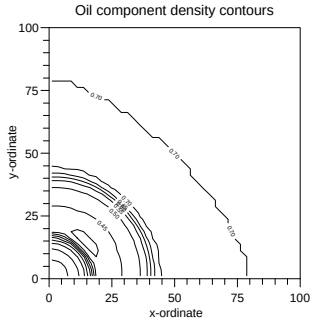
Oil component density contours
y-ordinate
x-ordinate
0
25
50
75
100
0.70
0.75
0.80
0.85
0.90
0.95

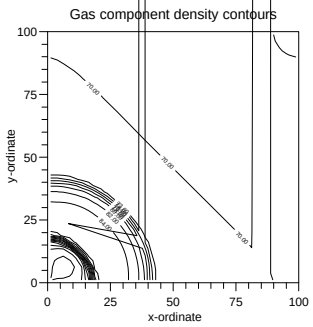
Gas component density contours
y-ordinate
x-ordinate
0
25
50
75
100
70.00
70.00
70.00

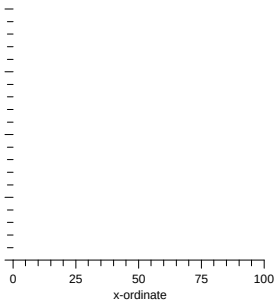
x-ordinate
0
25
50
75
100

for 3 days. Simulating the problem with the explicit treatment of the source at a lower CFL number would be prohibitively expensive even if the discrepancies were decreased. The results with the implicit treatment of the source are shown in Figure 5.25, with about 11-15 iterations needed to achieve convergence of the iteration (5.5.8) once the computation had settled down.

The two sets of results show a marked difference, which is due to the unacceptably large volume error discrepancies being generated in the results of the explicit treatment of the injection source term.

In 1-D the implicit treatment of the source term used to model injection of fluid into the reservoir has been shown to give improved results compared to an explicit treatment. No reduction of the CFL number is necessary with the implicit treatment. In 2-D the improvement when the implicit treatment is used is more apparent. The explicit treatment of an injection source produces unphysical results even at reduced CFL numbers. The implicit treatment of the source enables the simulation to generate reasonable results in terms of the magnitude of the volume error discrepancies and again can be run with a CFL number of 0.9.

In the next chapter we investigate the impact of the volume error discrepancy

Chapter 6

The Impact and Reduction of the Volume Error Discrepancy

6.1 Introduction

The work in this chapter concerns the volume error discrepancy associated with the splitting of the flow equations into hyperbolic and parabolic parts, namely equations (3.5.8) and (3.4.6). The resulting volume error discrepancy essentially indicates how well the equation of state, or volume balance equation, is satisfied in terms of pressure but more importantly indicates the error associated with the splitting methodology. These errors must therefore be kept as low as possible and controlled where necessary. In this chapter the impact of the volume error discrepancy is investigated as are two potential methods of reducing it.

The impact of the volume error discrepancy on the numerical results of reser-

and assessed in the next section of this chapter.

The system of conservation laws in the Black-Oil model are discretised to second order accuracy in both space and time whereas the pressure equation is only discretised to first order in time but having the same spatial accuracy. A formally

tain whether the same type of problem occurred and to offer possible remedies if needed.

6.2 Impact of the Volume Error Discrepancy

The impact of the volume error discrepancy on numerical results of reservoir simulations is assessed for 2-component 2-phase flow. The effect on the positioning and resolution of the fronts, if any, is of particular interest as is a general comparison of the results. The sequential (or split) solution methodology was first applied to 2-component 2-phase flow problems by Bell et al. [5], see Section 3.7. This model considers oil and gas fluid components and has a 'solution gas ratio' only, i.e.

both formulations. If this was not done then different amounts of diffusion would be introduced by the two methods and comparison of the results would not be so informative. It was found that the formulation of the model without the volume error discrepancy can be run with time steps calculated using the CFL criteria

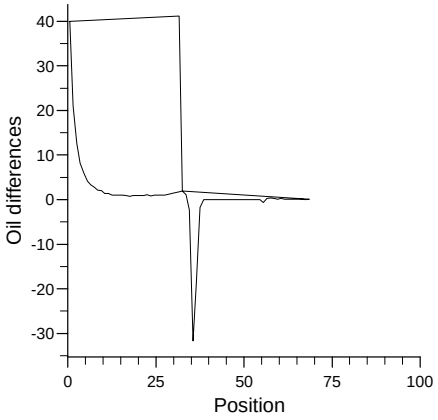
40
30
20
10
0
-10
-20
-30
Oil differences
0
25
50
75
100
Position

which would need to be solved by a non-linear iteration and thus would add considerable computational complexity since the coefficients in the equation would have to be updated every iteration. Trangenstein [49] justifies the reduced time accuracy by the fact that in secondary and tertiary recovery processes, which we are considering, the pressure field is slowly varying in time and hence the time truncation errors would not be expected to be too large. However a method does exist of obtaining second order time accuracy without the need of a non-linear iteration, d0Az7Bnon)Te'ffizffB7Sff7OC 0'z'B7Sff7OPedOiBiO'7i7Sff7e 7Sff7trAff 7ti'z Ltip

coefficients and the total velocities at the cell edges ( ) _ were evaluated at
the half time level in both (6.3.1) and (6.3.2), a Crank-Nicnze lnzeefficiezett7ASzLS) i07pBeOSz

and needs special consideration. This is because the Taylor series linearisation of the volume balance equation, used to derive the pressure equation, dictates that the volume discrepancy term in should be evaluated at the current time level rather than the half time level + – as in the corrector (6.3.5). Therefore the discrepancy term 1 must be treated as a constant and only the porosity term evaluated at the time level + – in the term in (6.3.5).

Douglas and Dupont point out that the dependent variable and the coefficients , , etc. in the parabolic equation must satisfy certain continuity and boundedness properties for the Galerkin formulation of the predictor corrector approach to achieve second order time accuracy. If the continuity property is not maintained for the coefficients in the pressure equation then a time accuracy of one and a half is obtained, i.e. (Δ^{-}), after the predictor corrector technique has been applied. Douglas and Dupont then state that a further pass through the corrector will achieve the desired second order time accuracy. In the finite difference case the continuity of the coefficients has a greater consequence on the ffi‘ff7in correcffi‘ff7irsffi‘ff7inc‘ff7in

The SOPC procedure was applied to both a saturated and undersaturated

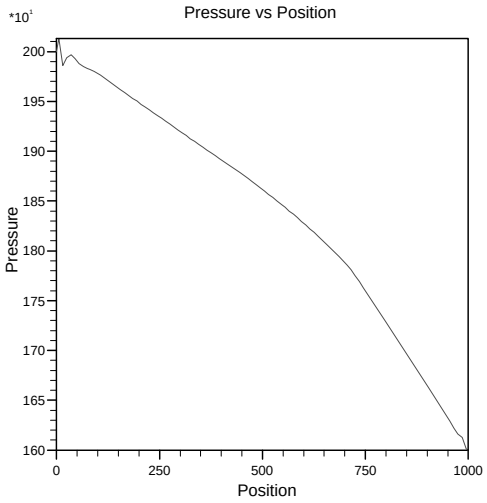

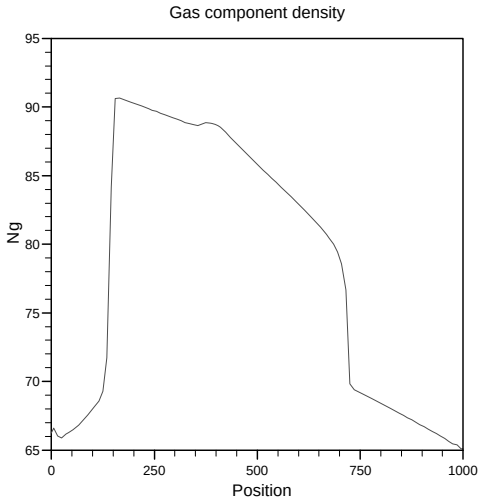

in 1-D the pressure equation can be solved by a direct method but in higher dimensions an iterative method must be used to solve the resulting linear system. The above percentage time for the 2-D pressure equation is based on using a typical engineering tolerance of 0.1 psi, and would obviously increase if lower tolerances were used. Therefore the SOPC technique is less viable in dimensions higher than 1, even if it had been found to have been successful at reducing the volume error discrepancy.

Since the SOPC technique was not found to reduce the volume error discrepancy an alternative method was devised, which is similar to the SOPC procedure, to try to reduce the volume error discrepancy. This simply involved repeating the pressure equation at the end of the time step, i.e. i.e.pLsSzffB0zffBvO aLOrsff7t peBssBp

6.4 Iterative Solution of the Volume Balance Equation

hoped to have the effect of substantially reducing the volume discrepancy errors. Controlling these errors is thought to be important in problems involving highly compressible fluids, such as steam in thermal simulations [48]. The volume error discrepancy also indicates the deviation in some sense of the numerical solution from the true physical solution behaviour, and so a high volume error discrepancy means that unacceptable errors have been introduced into the results. The results of test problems from [46] and those from [5] when run with the volume error discrepancy formulation, indicate that the highest volume discrepancies occur around phase changes. The errors are worse for problems involving 1-phase/2-phase fluid boundaries such as in the simulation problems from [5]. The reservoir model in [5] is a 2-phase (liquid, vapour), 2-component (oil, gas) model with a solution gas ratio ( ) only. In this formulation the volume balance equation amounts to a quadratic in pressure and hence can be solved exactly so that volume error discrepancies do not arise.

The pressure computed from the parabolic pressure equation is only approximate since the equation was obtained from the linearisation of the volume balance equation. A technique to improve on this was introduced in the following way. After solving the pressure equation and conservation laws these results were used

whilst for undersaturated flow with the vapour phase missing, $f(\mathbf{n}, p)$ becomes

$$f(\mathbf{n}, p) = \overline{B}_l(p, p_b)n_o + \overline{B}_a(p, p_b)n_w - 1,$$

and for undersaturated flow with the liquid phase missing

$$f(\mathbf{n}, p) = \overline{B}_v(p, \overline{R}_v)(n_g - R_a n_w) + B_a n_w - 1,$$

where, in this case, $\overline{R}_v$ is a function of pressure if water is present and gas is allowed to dissolve in the water.

The local iterative solution of the volume balance equation technique was first tried on problems 1 and 3 from [46] which are problems with no phase changes. Firstly problem 1 (which we have referred to as problem A2 and defined in Chapter 5) was simulated, using 100 grid blocks, with and without the volume error discrepancy reduction technique, with the maximum discrepancy errors being reduced from $\sim 10^{-4}$ to $\sim 10^{-10}$ with two iterations in each grid block. The two sets of results obtained look almost identical, so in Figure 6.4 we show the percentage differences between the two sets. Figure 6.4 indicates that the resulting

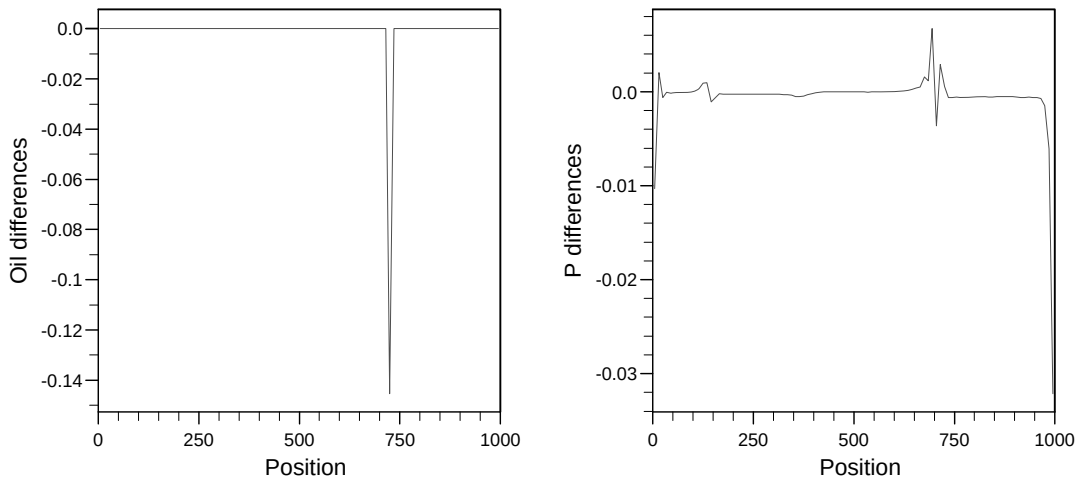

Figure 6.4: The percentage differences in the oil component density and pressure fields of problem A2, between the results of applying and not applying the discrepancy reduction technique.

corrected pressure field has very slightly shifted the second front in the problem.

The technique was then applied to an undersaturated flow problem, namely problem 3 from [46], (our reference A3 defined in Chapter 5), again with two

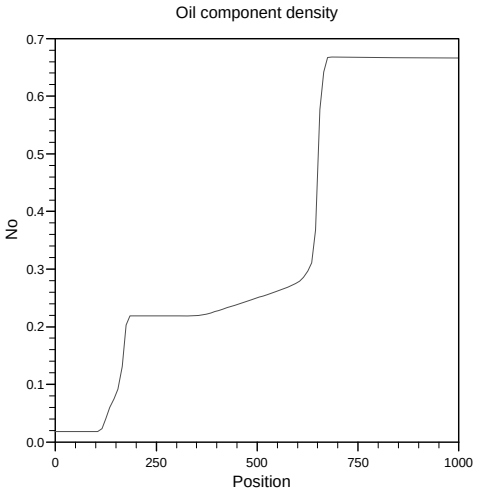
Oil component density
No
Position
0.0
0.1
0.2
0.3
0.4
0.5
0.6
0.7
0
250
500
750
1000

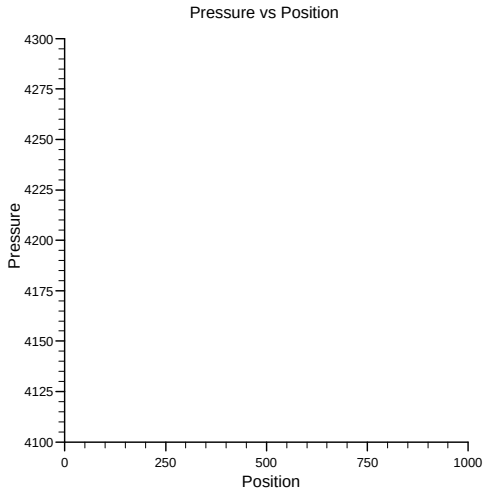
Pressure vs Position
Pressure
Position
4100
4125
4150
4175
4200
4225
4250
4275
4300
0
250
500
750
1000

The technique is also successful for problems with phase changes when the modification just described is applied, i.e. solving the volume balance equation with respect to component density rather than pressure at the phase changes. However the modification of the component density vector by iterating on the volume balance equation has a consequence in that conservation of mass is not maintained at these points. But the modification of the vector to reduce the volume error discrepancy is usually small, namely less than 1.0 . Therefore loss of conservation of mass at the phase changes does not seem to pose a problem due to this small correction and since the results obtained in the process are qualitatively as before, the volume error discrepancy having been reduced substantially.

When the iteration on the volume balance equation is performed it is possible to reduce the discrepancy errors to below 10 , usually much lower. In such a case it is not unreasonable to assume that the volume balance equation is satisfied in terms of machine accuracy and hence exactly which means that p and would not be independent, as mentioned in Section 3.6. Hence the effect of — should be included in the characteristic analysis, whereas at present it is assumed — = 0. This would mean the characteristic analysis would have to be reformulated which is not within the scope of this thesis.

The method of reducing the volume error discrepancy described in this section was tried on the 2-component 2-phase problem from Section 6.2, (problem A1), which was used to compare the formulations of the method with and without the volume error discrepancy. This was done to assess the success of the technique to reduce the volume error discrepancy and hence whether its application leads to more physically accurate results, like those from the formulation with no volume error discrepancy. The reservoir problem in question exhibits two phase changes over the length of the reservoir, an undersaturated region lies between two saturated fluid regions. Hence the component density vector will be corrected instead of pressure at the phase changes. The results of this simulation are shown in Figure 6.10, all parameters being the same as in Section 6.2. These results are in closer agreement to those results from the no volume error discrepancy formulation shown in Figure 6.1 compared to those from the volume error discrepancy formulation without the discrepancy reduction also shown in Figure

6.1, we justify this statement below.

Although the three sets of results look very similar, tests on the norms of the differences between the solution values indicate that the results of applying the discrepancy reduction techniques gives results closer to those from the no volume error discrepancy formulation and hence more physically accurate results. We calculated both the 1 and 2-norms and found these both to have been reduced for course (50 blocks) and fine (100 blocks) grid simulations when the technique was used. The improvement being greater as the grid was coarsened. In Figure 6.11 we again show the percentage differences between the results without the volume error discrepancy (Figure 6.1) and with the discrepancy reduction (Figure 6.10).

and component density fields in the case of mixed flow problems, will need a greater correction. However the volume error discrepancy reduction technique

6.5 Effect of Increased Fluid ompressibility

The compressibility of each fluid component is given by

$$c_f = \frac{1}{\rho}\frac{\partial \rho}{\partial p} = B\frac{\partial}{\partial p}\left(\frac{1}{B}\right),$$

where p is the pressure, ρ is the density and B is the formation volume factor. Throughout this section we drop the negative sign associated with compressibility to simplify the discussion. We now derive expressions for the compressibilities of gas from the Black-Oil model and steam from the thermal model in order to compare the two. In the Black-Oil model the vapour formation volume factor is given by

$$B_v(p) = \frac{1}{(6 + 0.06p)}, \tag{6.5.7}$$

therefore the vapour compressibility is

$$c_v(p) = \frac{0.06}{(6 + 0.06p)}.$$

The steam density function is given by different functional forms over the pressure range, i.e.

$$\left(\frac{p}{p_b}\right)\frac{1}{\rho_v(p)} = \begin{cases} \frac{490.386}{p} & 0.04703 \quad \text{if } p \quad 1500 \text{ psi} \\ \frac{551.74}{p} & 0.0887 \quad \text{if } p > 1500 \text{ psi} \end{cases},$$

where ρ_v is the steam (vapour) density in lb ft^{-3}, p is the pressure and p_b is the bubble point pressure which is a function of the temperature. This is of the general form

$$\rho_v(p) = \frac{p^2}{p_b(a \quad bp)}, \tag{6.5.8}$$

where a and b are the constants above depending on which pressure interval p is in. The compressibility of steam in the thermal simulations is therefore given by

$$c_s(p) = \frac{2a \quad bp}{p(a \quad bp)}.$$

The compressibilities of steam from the thermal model and gas from the Black-Oil model are shown graphically in Figure 6.12, the steam compressibility can be seen to be an order of magnitude higher than that of the gas over most of the pressure range. The discontinuity in the steam compressibility is because the first derivative of $\rho_v(p)$ is discontinuous although $\rho_v(p)$ is continuous to only 3 decimal places.

In order to examine the effect of increased fluid compressibility within the Black-Oil model one of the fluid compressibilities must be increased. Gas is the most compressible fluid component in the Black-Oil model therefore it would be natural to try to increase the compressibility of the gas to match that of steam. A gas compressibility to match that of steam cannot be found by altering the parameters in (6.5.7). Instead a density function similar in form to (6.5.8) was converted into a formation volume factor for use in the Black-Oil model, the parameters used to accomplish this were $a = 450.0$ and $b = 0.09$. The resulting

gas compressibility compared to that of steam is shown in Figure 6.13 and can be seen to be just greater than that of steam throughout the pressure range.

A problem was devised which has a large variation in compressibility, namely gas injection into an oil saturated reservoir, therefore we have a 2-component, 2-phase problem. This type of problem gives a compressibility difference of 2 orders of magnitude between the injected and initial reservoir fluid. The mass transfer ratio $R_a \equiv 0$ since there is no water in the problem, the ratios R_l and R_v were also set to zero because no mass transfer effects were modelled in the thermal model. The absence of mass transfer effects in the Black-Oil model also ensures that the variation in compressibility occurs over a very narrow region, i.e. about 3 or 4 grid blocks, as would be expected in the thermal model.

A CFL number of 0.9 was used for this computation, after a few days into the simulation large volume error discrepancies were generated which caused oscillation in the pressure and component density fields. The same time as the large volume error discrepancies were generated the time steps being used were increasing to about 7 days which was much larger than those previously seen in Black-Oil computations performed thus far. Therefore this suggests that the wavespeeds in the problem were not being sampled well by the numerical method and the time steps calculated using the CFL criteria were unstable. xperience with Black-Oil computations has shown that unstable time steps can be responsible for generating large volume error discrepancies which cause unphysical oscillations in the results. The simulation was repeated using a CFL number of 0.5 and run to a late time, i.e. time for the front in the problem to have nearly reached the producer. The results obtained were free of any oscillation, the simulation proceeding smoothly, no large volume error discrepancies being generated. In particular no problems such as backflow in the pressure equation were observed. The maximum volume error discrepancies generated were of the order 10^{-3} to 10^{-4} with an occasional discrepancy of order 10^{-2}.

Further investigation showed that the large discrepancies occurred at the location of a shock in a rarefaction-shock compound wave. An entropy violation also occurred at this point, therefore extra numerical dissipation was needed at this point which was provided by the CFL number reduction of 0.9 to 0.5. A

local addition of dissipation to improve entropy satisfaction at this point may also be provided by decreasing the slope limiting parameter gamma in (4.2.4) to 1.0 when a local linear degeneracy is detected rather than using = 1 5. The problem was repeated with the above modification to the algorithm with a CFL number of 0.9 and also limiting the increase of time steps to a maximum of 20 as

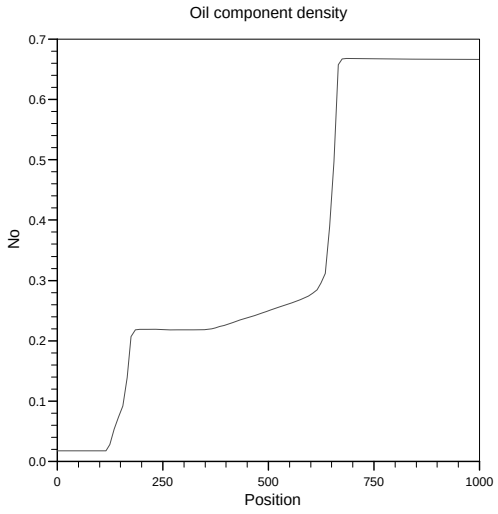
Oil component density
No
Position
0.0
0.1
0.2
0.3
0.4
0.5
0.6
0.7
0
250
500
750
1000

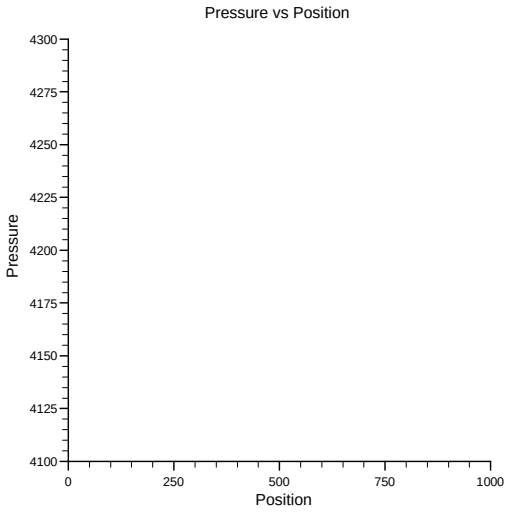
Pressure vs Position
Pressure
Position
4100
4125
4150
4175
4200
4225
4250
4275
4300
0
250
500
750
1000

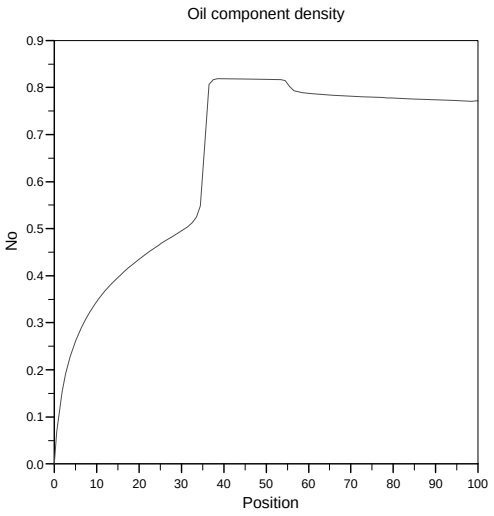
Oil component density
No
Position
0.0
0.1
0.2
0.3
0.4
0.5
0.6
0.7
0.8
0.9
0
10
20
30
40
50
60
70
80
90
100

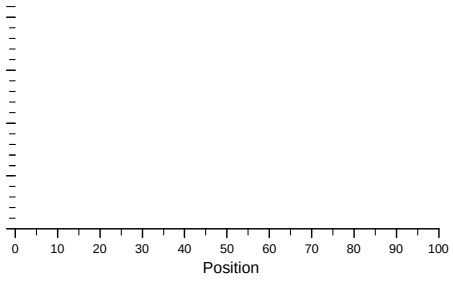
Position
0
10
20
30
40
50
60
70
80
90
100

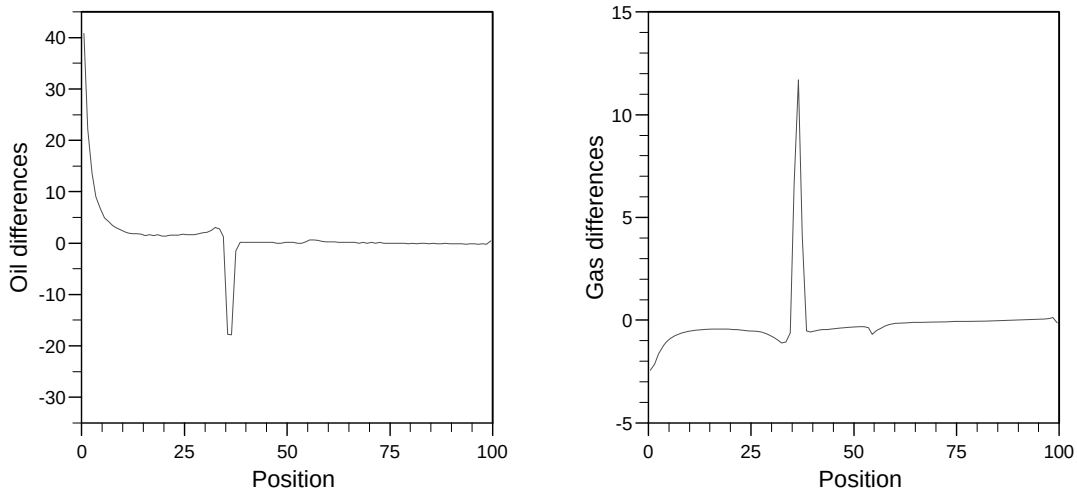

Figure 6.11: The percentage differences between the oil and gas component densities from problem A1 without the volume error discrepancy and with the discrepancy but the discrepancy reduction techniques having been applied.

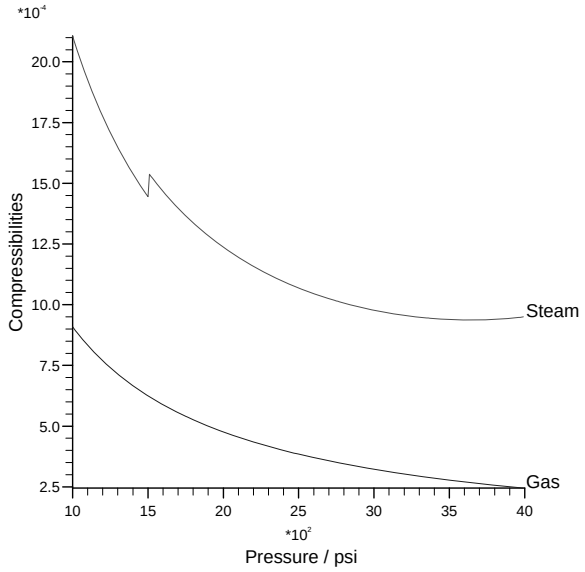

Figure 6.12: The steam and gas compressibilities, having units of psi^{-1}, used in the thermal and Black-Oil model respectively.

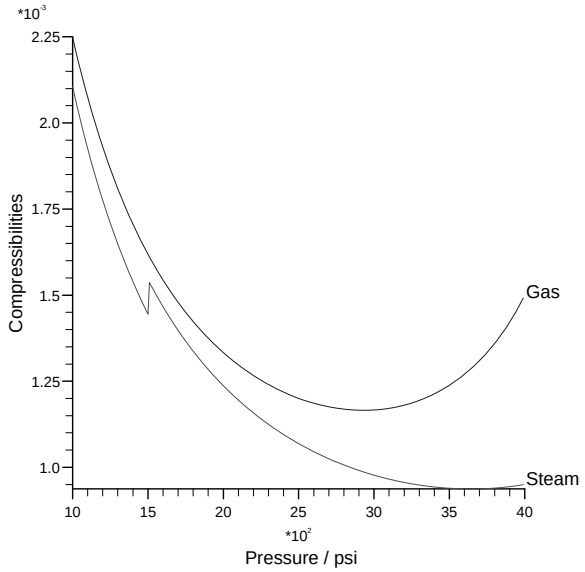

Figure 6.13: The increased gas compressibility, used in the Black-Oil model to simulate the injection of highly compressible fluid.

Chapter 7

A Comparison of TVD Flux-Limiter and Higher Order Godunov Schemes for Reservoir Simulation

7.1 Introduction

In this chapter we compare the numerical performance of the Higher Order Godunov scheme [2] and a TVD flux-limiter scheme, developed at B.P. Sunbury by Rubin and Edwards [36], when applied to the system of degenerate conservation laws arising from the Black-Oil flow equations. The Higher Order Godunov

Flux-limiter schemes were constructed with non-degenerate systems of conservation laws in mind, see [7, 36, 45] for details, i.e. systems that possess genuinely non-linear (or linearly degenerate) wave modes and that are strictly hyperbolic in nature. The Higher Order Godunov methodology was also originally developed for non-degenerate systems by Collela [10], with Bell et al. [2] presenting extensions of Collela's work enabling the scheme to be applied to degenerate systems, specifically those with local linear degeneracies and eigenvector deficiencies. The flux-limiter scheme in VIP does not rely on any knowledge of the characteristic structure of the conservation laws, i.e. it does not decompose the system into its characteristic components, and hence no clear mechanism exists of detection of the degeneracies and modification of the scheme. This is in contrast to the Higher Order Godunov methodology since the same characteristic information used to construct the scheme can also be used to test for the degeneracies. However since the characteristic information is used to construct the scheme, then suitable modifications to the scheme at degeneracies are now made a necessity.

Timings of individual subroutine calls in the Higher Order Godunov code indicate that the calculation of the eigenvectors can represent a significant amount of the total computational time, i.e. over 5 , in both 1 and 2 dimensions. The eigenvectors being used in the construction of second order accurate traced left and right states at cell interfaces, see Section 4.2.2. The eigenvectors are also used in the phase space construction needed to solve the Riemann problem at cell edges, see Section 4.2.3, and arises in problems in which counter-current flow occurs, due to the introduction of gravitational effects. However the relative computational time, associated with the calculation of the eigenvectors, decreases when gravity is introduced. This is because, although more eigenvector calculations will be needed compared to problems without gravity, extra computations are associated with introducing gravity, especially in solving the Riemann problems to compute the numerical fluxes. The timings indicate that in terms of calculating the eigenvectors, the most efficient problems are the 2-D cross-sectional problems, with the gravity-free 1-D problems the least efficient.

flux-limiter schemes have to be used with lower CFL numbers, the greatest being 0.66 but usually 0.5, depending on the limiter used. But we have found that when problems involving counter-current flow are being simulated with the Higher Order Godunov code a reduced CFL number in the range 0.5-0.9 is needed for best performance of the method.

7.2 Description of the VIP Simulator

the fluid pressure and the vapour and aqueous saturations, and respectively. The three mass conservation laws are then discretised with a backward in

each wave mode, i.e.

$$= \bar{} \bar{}$$

where the matrix $\bar{}$ is the matrix of eigenvectors evaluated at an expansion state $\bar{}$, i.e. $\bar{} = \quad (\bar{})$. We have a system of 3 conservation laws and therefore the jump will be decomposed into 3 components or separate paths. If the eigenvectors (columns of $\bar{}$) are normalised, the entries of $\bar{}$ represent the lengths of the paths in phase space. The expansion state $\bar{}$ is calculate as an average of the traced left and right component densities, which define the Riemann problem at cell interfaces, i.e.

$$\bar{} = \frac{1}{2}(\quad + \quad)$$

Alternative expansion states are possible but the above form is recommended in [2] for problems involving flow in porous media.

The inherent volume error discrepancy associated with the flow equations can

$$\bar{}$$

$$\bar{}$$

$$\bar{} \quad \bar{}$$

$$\bar{} \bar{}$$

$$\bar{} \bar{}$$

taking less than half the percentage time compared to before.

Given the percentage times above, it should be noted that the Higher Order Godunov code was not written with efficiency in mind, but was coded as efficiently as possible. In particular, we used a BI-CGSTAB pre-conditioned conjugate gradient solver, described by Van Der Vorst [53], to solve the linear system resulting from the 2-D parabolic pressure equation, so that this step of the computation is of high efficiency. We tried using optimisation of the Higher Order Godunov code, with the effect on the percentage timings mostly being within ± 2 of those quoted.

Percentage timings of the calculations of the eigenvectors have been given, but these do not take into account the extra computation associated with performing the eigenvector decomposition. For instance we need to solve 3 $n \times n$ linear systems in each grid block to calculate the expansion coefficients (4.2.2), used in the calculation of the monotonised slopes, see Section 4.2.1, and a $n \times n$ linear system associated with the Riemann problem solution, where n is the number of conservation laws in the system. Taking into account all the computation associated with a full eigenvector decomposition, used in the Higher Order Godunov scheme, it is concluded that the time spent in performing these computations is significant and perhaps should be justified in terms of quality of numerical results compared to the flux-limiter schemes, which do not require the same computational effort.

7.4 omparison of Numerical Results

In this section we show the numerical results from the Higher Order Godunov code and the VIP simulator to compare how well the numerical schemes handle the Black-Oil fluid flow equations. We show results of a 1-D and 2-D Areal problem which do not include gravitational effects, and a 2-D cross-sectional problem which does include gravity. The 2-D cross-sectional problem introduces counter-current fluid flow and hence will be a good test of the numerical methods, particularly the Higher Order Godunov method since all aspects of the scheme will be utilised. Also in this problem it is likely that points of a loss of strict hyperbolicity will occur and hence the modifications present in the Godunov

We now describe the 1-D simulation problem used to compare the two approaches to solving the Black-Oil flow equations. The reservoir modelled was 500 feet in length and had a rock permeability of 100 milliDarcy's. The injection fluid consists of water and gas at a pressure of 2000 psi and had saturations of

$$\mathbf{s}_{inj} = \begin{bmatrix} 0.0 \\ 0.2235 \\ 0.7765 \end{bmatrix}.$$

The fluid initially resident in the reservoir was at a pressure of 1800 psi and had a composition of

$$\mathbf{s}_{res} = \begin{bmatrix} 0.7658 \\ 0.1406 \\ 0.0936 \end{bmatrix},$$

with the production pressure being 1600 psi. All the other reservoir, fluid and rock parameters are the same as those given in Section 3.9. We reiterate that the mass transfer ratios R_v and R_a are both identically equal to zero for all the reservoir simulations in this chapter. The results of this simulation problem from the VIP code at 30 days using 100 grid blocks, and with a CFL number of 0.5, are shown by the solid line in Figure 7.1. The tolerance used to solve the pressure equation for these results was an absolute value of 0.1 psi, representing 5 figure accuracy, i.e. pressure in every grid block was calculated to a tolerance of at worst 0.1 psi. The corresponding results from the Higher Order Godunov code, with the direct solution of the linear system resulting from the discretisation of the pressure equation, are shown by the crosses in Figure 7.1. We note that the IMP S formulation of the flow equations does not have an inherent volume error discrepancy therefore we could have applied the techniques, described in the previous chapter, to reduce the volume error discrepancy, to see the effect on the comparison. However at a CFL number of 0.5 the maximum volume error discrepancies generated are $O(10^{-5})$ therefore applying the techniques, although reducing the volume error discrepancy, do not noticeably effect the results, therefore we do not show the results of this computation.

In comparison of the results we see that the rarefaction stretching from about 10 to 110 feet is resolved almost identically by the two codes. However the

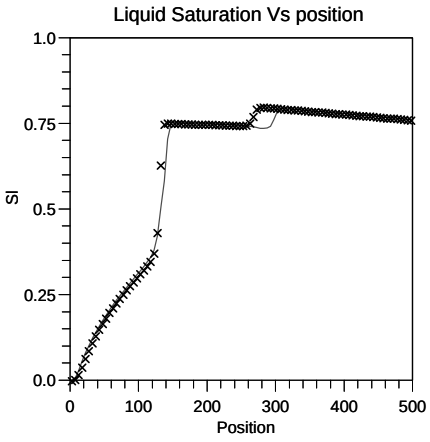
Liquid Saturation Vs position
Sl
1.0
0.75
0.5
0.25
0.0
0
100
200
300
400
500
Position

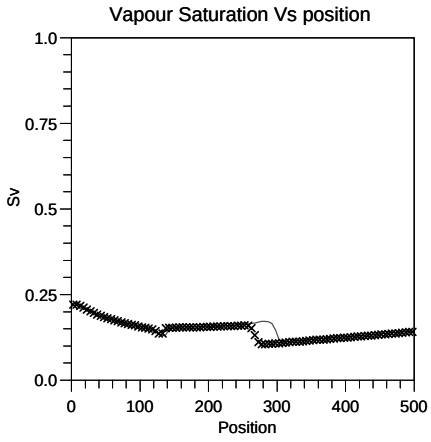
Vapour Saturation Vs position
Sv
1.0
0.75
0.5
0.25
0.0
0
100
200
300
400
500
Position

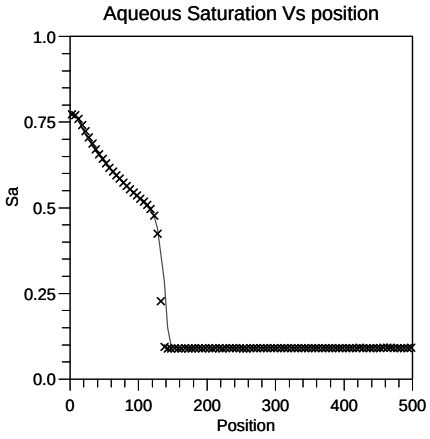
Aqueous Saturation Vs position
Sa
1.0
0.75
0.5
0.25
0.0
0
100
200
300
400
500
Position

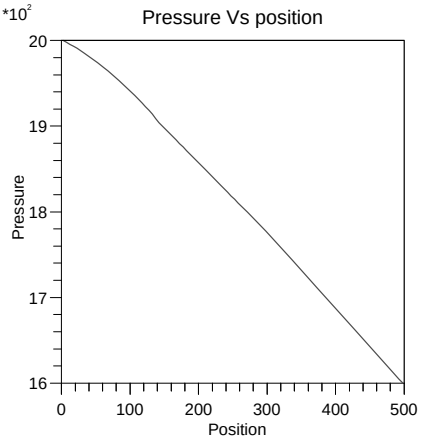
*10^2
Pressure Vs position
Pressure
20
19
18
17
16
0
100
200
300
400
500
Position

Therefore the discrepancy in the location of the second shock is probably due to the different mass fluxes injected early on in the computation, with conservation of mass ultimately causing the differences. A similar kind of effect on 'the faster shock' was also observed in computations performed by Blunt and Rubin in [7]. The Higher Order Godunov code takes 146 time steps whereas the VIP code takes 2479 time steps to perform the simulation. Hence the Higher Order Godunov code is far more efficient at performing the simulation.

The 2-D Areal problem was simulated on a 100 feet square region with a rock permeability of 100 milliDarcy's in both coordinate directions. The injection, initial reservoir and production pressures were 2000,

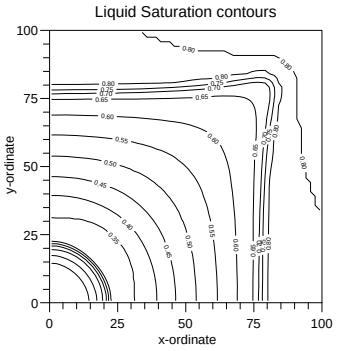
Liquid Saturation contours
y-ordinate
x-ordinate
0
25
50
75
100

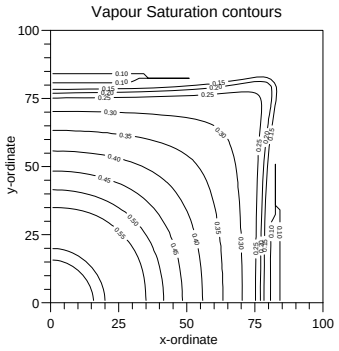
Vapour Saturation contours
y-ordinate
x-ordinate
0
25
50
75
100

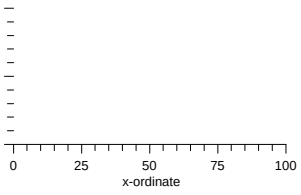
x-ordinate
0
25
50
75
100

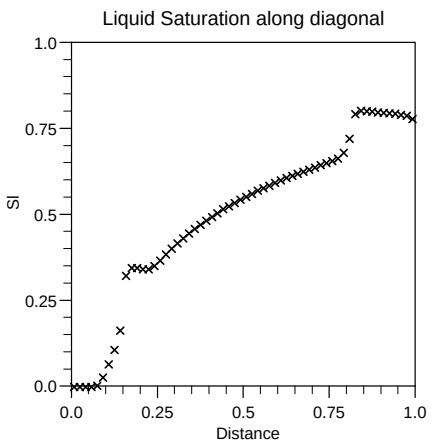
Liquid Saturation along diagonal
Sl
Distance
1.0
0.75
0.5
0.25
0.0
0.0
0.25
0.5
0.75
1.0

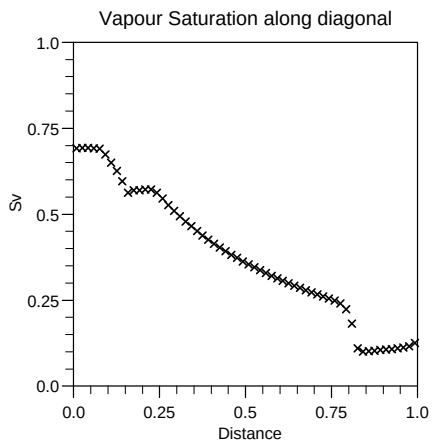
Vapour Saturation along diagonal
Sv
Distance
1.0
0.75
0.5
0.25
0.0
0.0
0.25
0.5
0.75
1.0

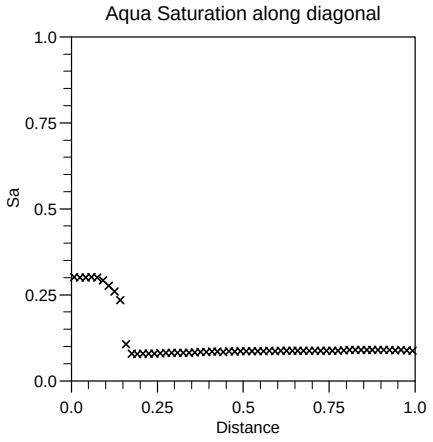
Aqua Saturation along diagonal
Sa
Distance
1.0
0.75
0.5
0.25
0.0
0.0
0.25
0.5
0.75
1.0

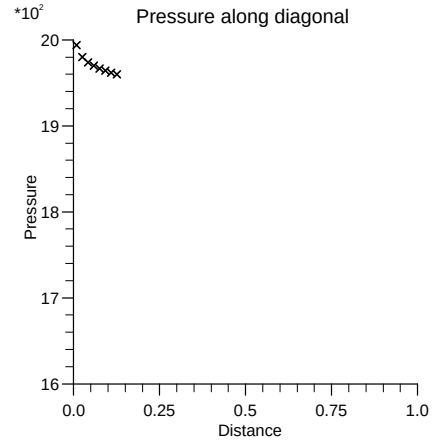
*10^2
Pressure along diagonal
Pressure
Distance
20
19
18
17
16
0.0
0.25
0.5
0.75
1.0

larger magnitude, which is possibly due to the inherent volume error discrepancy.

with the vertical. When the fluid only contains 1 phase the required pressure gradient in the reservoir is the pressure gradient associated with that phase

$$— = —$$

However when more than 1 phase exists we use a saturation weighted average of the individual pressure gradients associated with each phase, i.e.

$$— = — + — + —$$

The injected fluid had a composition of the following saturations,

$$\begin{matrix} & 0\ 0 \\ = & 0\ 0 \\ & 1\ 0 \end{matrix}$$

i.e. a waterflood, with a pressure at the top of the injection face of 2000 psi, the pressures were distributed down the the rest of the face using the pressure gradient — associated with the injected fluid. The initial reservoir saturations were

$$\begin{matrix} & 1\ 0 \\ = & 0\ 0 \\ & 0\ 0 \end{matrix}$$

with the pressure along the top of the reservoir being 1800 psi and the pressures below being distributed with a similar procedure to the injection face. Although there is no free gas initially in the reservoir, due to the vapour saturation being zero, there is an amount of gas dissolved in the oil as indicated by the 'solution gas ratio' and hence the initial reservoir fluid is undersaturated. A production pressure of 1600 psi was assigned along the whole production face. The vector of phase densities, at standard conditions, used in this problem were

$$\begin{matrix} & 52\ 789 \\ = & 0\ 07655 \end{matrix}$$

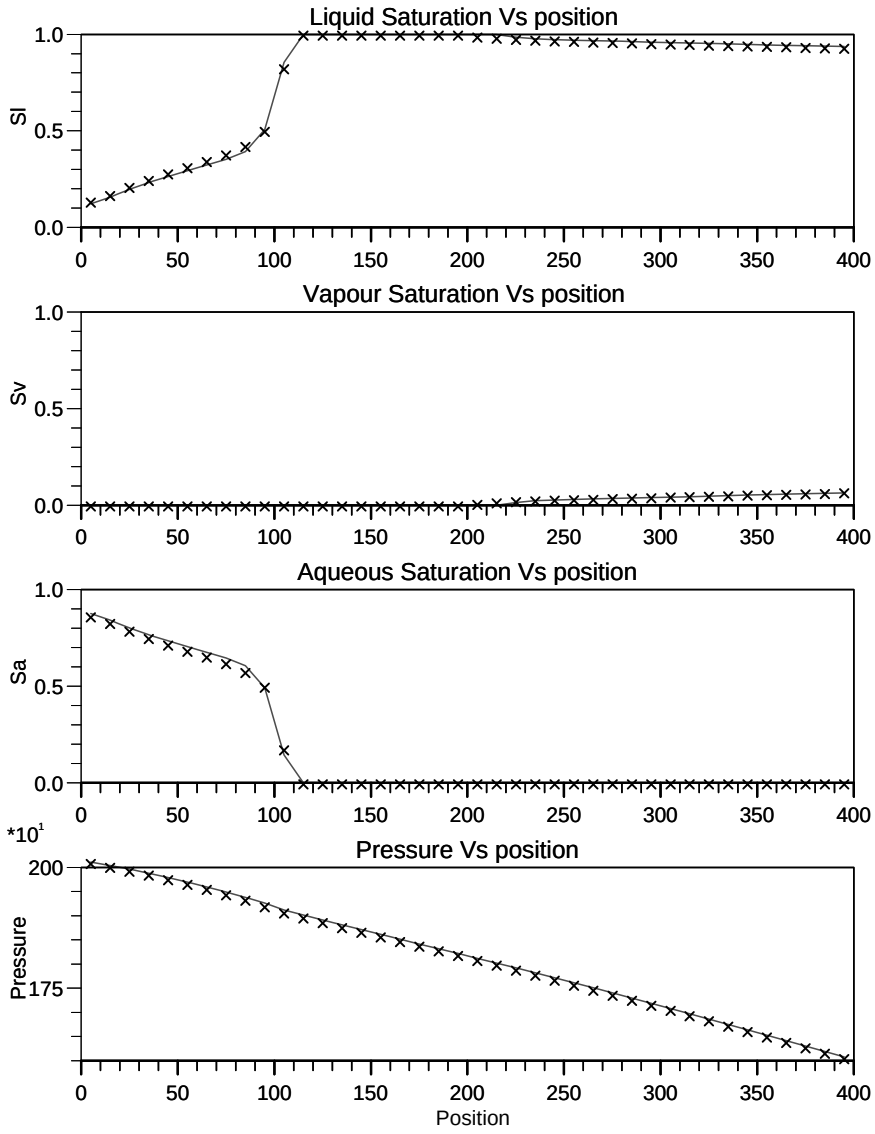

Figure 7.7: Numerical results of the 2-D cross-sectional problem from the VIP and Higher Order Godunov codes along the middle of the reservoir overlaid, taken at 15 days using a 40 20 grid and a CFL number of 0.5, solid line - VIP, crosses - Higher Order Godunov code.

Comparison of numerical results from the VIP and Higher Order Godunov codes in 1 and 2-dimensions has exhibited some notable differences. Firstly the VIP code predicted a more advanced position of the second shock front in the

in the computations, caused by the uncertainty about the injection well model used in the VIP code, and would seem to be confirmed by the results from the cross-sectional problem.

Secondly, the 2-D Areal results from the VIP code indicate that it has failed to resolve the prescence of a rarefaction wave in a rarefaction-shock compound wave near the injection well. The Higher Order Godunov code captures this compound wave, with an analogous 1-D problem confirming its existence. In general the two codes exhibit similar resolution of rarefaction waves and constant states, with improved shock resolution from the Higher Order Godunov code. Unfortunately we were unable to obtain results from VIP of the 2-D Areal problem at an earlier time to compare the resolution of the second shock front. With regard

is used), the Higher Order Godunov code has a theoretical stability limit of a CFL number of 1.0. The number of time steps used to perform the simulations has confirmed the Higher Order Godunov code is far more efficient in terms of overall computational time. Hence the superior resolution and overall efficiency of the Higher Order Godunov code compared to the VIP code, justify use of a full eigenvector decomposition in the algorithm.

Chapter 8

Summary and Further Work

In this thesis we have investigated the high resolution simulation of compressible fluid flow in oil reservoirs. In particular the Higher Order Godunov method has

also discussed the solution of the parabolic pressure equation. We showed results from our 1-D code and compared them with results in the literature thereby validating our code. The 2-D code was validated by comparison of results with those from a commercial reservoir simulator.

Also in Chapter 5 the accuracy of the Higher Order Godunov method was investigated by applying it to the degenerate system of conservation laws arising from the 3-phase incompressible Buckley-Leverett model, see [49], for which we also constructed analytic solutions, and thus were able to compare the analytic and numerical results. The agreement of the numerical results with the analytic constructions was found to be very good.

Finally in Chapter 5, source terms were incorporated to model injection and production of fluid in 1 and 2 dimensions. A locally implicit procedure was used to remove the numerical stability problem associated with their use. The approaches described were effective at modelling source terms in 1 and 2 dimensions, and exhibited improved results over an explicit treatment.

The work in Chapter 6 concerned the inherent volume error discrepancy associated with the 3-component 3-phase Black-Oil model [46]. A 2-component 2-phase Black-Oil model [5] also exists, being the forerunner to the Black-Oil model [46], which was developed by Bell et al. and does not have an associated volume error discrepancy. Therefore 2-component 2-phase reservoir simulations may be performed with and without the volume error discrepancy and hence the effect of the discrepancy on the numerical results was investigated. We found that the results of these reservoir simulations were in close agreement and hence conclude that the Black-Oil model with the inherent volume error discrepancy is a good approximation to the more physically accurate Black-Oil model [5], at least for 2-component 2-phase simulations.

Also in Chapter 6 we investigated the application of a Second Order Pressure

present in the commercial reservoir simulation code VIP were compared to those from the Higher Order Godunov scheme, when applied to the degenerate system of conservation laws arising from the Black-Oil model. We discussed the relative efficiencies of the two numerical schemes and compared the quality of the numerical results.

The VIP code has an advantage over the Higher Order Godunov code since the TVD scheme is easily implemented component by component to the system of conservation laws. However this leads to a disadvantage of the scheme in that the resolution obtained is not as high as that obtainable from the Higher Order Godunov code, which is due to the ignoring of the coupling of the equations, and was shown in the comparisons of the numerical results. Another disadvantage of the VIP code is that it must be used with a CFL number of 0.5, whereas the Higher Order Godunov scheme can theoretically be used with a CFL number of 1.0. Also in practice the Higher Order Godunov code takes far fewer time steps to perform the simulations and hence is far more computationally efficient. It is therefore felt that these points justify use of the full eigenvector decomposition in the Higher Order Godunov code.

8.2 Further Work

We now discuss some ideas for further work, the most obvious being the use of adaptive gridding techniques for solution of the partial differential equations. The main idea here is to concentrate the computational effort where the solution to the conservation laws is changing most rapidly, with a relatively course grid where the solution is not changing with time. Hence improved resolution is obtained at discontinuities and savings in computational effort result. However adaptive gridding techniques have been applied to 2-D polymer flooding and 2-D 2-phase incompressible flow, using the Higher Order Godunov method, by dwards [16], but not to 3-phase compressible flow. In particular dwards presents a formulation giving high quality results on large aspect ratio grids.

The ultimate goal here is the construction of a 3-D adaptive strategy, and hence a computer code, to solve the Black-Oil flow equations in the most efficient

way possible. Grid adaptivity introduces an interesting problem in that the rock properties need to be held on the finest computational grid, and hence some sort of averaging procedure of the properties is needed in order to be able to represent them on the coarser grids. One way of tackling this problem is known as 'renormalisation', see King [27]. dwards and Christie [17] have shown how this renormalisation technique can be combined with an adaptive Higher Order Godunov scheme in 2-D.

Another area of further work involves the discretisation used in the parabolic pressure equation. The largest volume error discrepancies generated in the numerical results occur at phase changes and discontinuities in the component density field. The coefficients in the pressure equation at the cell edges are calculated by averaging the coefficients either side of the cell interface, which could be in between a phase change or part of a discontinuity. Therefore this averaging out of the coefficients could have a bearing on the relatively high volume error discrepancies generated at the phase changes and discontinuities. This could be investigated, as could modifications to the discretisation of the pressure equation to improve the situation, if it is found to be a cause. Hence this could represent a correction of the root cause of the high discrepancies at the said points, rather than the correction of the discrepancies once they have arisen.

[9] M.A.Christie and D.J.Bond, "Multidimensional Flux-Corrected Transport for Reservoir Simulation" in ighth SP Symposium on Reservoir Simulation, pp 81-90, Dallas, Texas, Feb 1985.

[10] P.Collela, "Multidimensional Upwind Methods for Hyperbolic Conservation Laws", J. Comp. Phys. **87**, pp 171-200, 1990.

[11] P.Collela and P.Woodward, "The Piecewise Parabolic Method (PPM) for Gas-Dynamical Simulations", J. Comp. Phys. **54**, pp 174-201, 1984.

[12] J.P.Collins, P.Collela and H.M.Glaz, "An Implicit- xplicit ulerian Godunov Scheme for Compressible Flow", submittted to J. Comp. Phys. 1990.

[13] R.Courant, K.Friedrichs and H Lewy, Mathematische Annalen, **100**, p 32, 1928.

[14] .C.Donaldson, G.V.Chilingarian and T.F.Yen, " nhanced Oil Recovery, II Processes and Operations", lsevier Science Publishers, Amsterdam, 1989.

[15] J.Douglas and T.Dupont, "Galerkin Methods for Parabolic quations", SIAM J. Numer. Anal. **7**, pp 575-626, 1970.

[16] M.G. dwards, "A Dynamically Adaptive Godunov Scheme for Reservoir Simulation on Large Aspect Ratio Grids", To Appear in the Proceedings of the ICFD Conference on Numerical Methods for Fluid Dynamics, University of Reading 1992.

[17] M.G. dwards and M.A.Christie, "Dynamically Adaptive Godunov Schemes with Renormalization in Reservoir Simulation", SP paper 25268, in Proceedings of the 12th SP Symposium on Reservoir Simulation, New Orleans, 1993.

[18] B. ngquist and S.Osher, "Stable and ntropy Satisfying Approximations for Transonic Flow Calculations", Math. Comp. **34**, pp 45-75, 1980.

[19] B. ngquist and S.Osher, "One Sided Difference Approximations for Nonlinear Conservation Laws", Math. Comp. **36**, pp 321-351, 1981.

[20] S.K.Godunov, "A Finite Difference Method for the Numerical Computation of Discontinouous Solutions of the quations of Fluid Dynamics", Mat. Sb. **47**, pp 271-290, 1959.

[21] G.H.Golub and C.F. van Loan, "Matrix Computations", John Hopkins University Press, 1983.

[22] J.Goodman and R.LeVeque, "A Geometric Approach to High Resolution TVD Schemes", SIAM J. Numer. Anal. **25**, pp 268-284, 1988.

[23] J.Goodman and R.LeVeque, "On the Accuracy of Stable Solutions for 2D Scalar Conservation Laws", Mathematics of Computation **45**, pp 15-21, 1985.

[24] A.Harten, "High Resolution Schemes for Hyperbolic Conservation Laws", J. Comp. Phys. **49**, pp 357-393, 1983.

[25] A.Harten, P.D.Lax and B. Van Leer, "On Upstream Differencing and Godunov Type Schemes for Hyperbolic Conservation Laws", SIAM Review, **25**, pp 35-67, 1983.

[26] K.Holing, J.Alvestad and J.Trangenstein, "The Use of Second Order Godunov Type Methods for Simulating OR Processes in Realistic Reservoir Models", in proceedings of the second uropean Conference on the Mathematics of Oil Recovery, ditions Technip, Paris, pp 101-111, 1990.

[27] P.R.King, "The use of Renormalisation for Calculating ffective Permeability", Transport in Porous Media, **4**, pp 37-58, 1989.

[28] P.D.Lax, "Hyperbolic Systems of Conservation Laws and The Mathematical Theory of Shock Waves" SIAM Regional Conference Series in Applied Mathematics, 1973.

[29] P.D.Lax and B.Wendroff, "Systems of Conservation Laws", Comm. on Pure and Applied Math. **13**, pp 217-237, 1960.

[30] T.P.Liu, "The Riemann Problem for General Systems of Conservation Laws", J. Diff. qns. **18**, pp 218-234, 1975.

[31] O.A.Oleinik, "Discontiuous Solutions of Non-linear Differential quations", Amer. Math. Soc. Transl. Ser. , , pp 95-171, 1957.

[32] S.Osher and F.Solomon, "Upwind Difference Schemes for Hyperbolic Systems of Conservation Laws", Math. Comp. , pp 339-374, 1982.

[33] P.Roe, "Approximate Riemann Solvers, Parameter Vectors and Difference Schemes", J. Comp. Phys. , pp 357-372, 1981.

[34] P.Roe, in proceedings of Large Scale Computations in Fluid Mechanics, "Some Contributions to the Modelling of Discontinuous Flows", Lecture Notes in Applied Maths., , part 2 pp 163-193, AMS, 1985.

[35] P.Roe and D.Sidilkover, "Optimum Positive Linear Schemes for Advection in Two and Three Dimensions", SIAM J. Numer. Anal. , pp 1542-1568, 1992.

[36] B.Rubin and M. dwards , " xtension of the TVD Midpoint Scheme to Higher Order Accuracy", SP paper 25265, in Proceedings of the 12th SP Symposium on Reservoir Simulation, New Orleans, 1993.

[37] V.V.Rusanov, "Calculation of Interaction of Non-Steady Shock Waves With Obstacles", J. Comput. Math. Phys. USSR, , pp 267-279, 1961.

[38] D.Schaeffo

[42] H.L.Stone, "Probability Model for stimating Three-Phase Relative Permeability", J. Pet. Tech. , pp 214-218, 1970.

[43] H.L.Stone and A.O.Garder, Jr., "Analysis of Gas-Cap or Dissolved Gas Reservoirs", Trans. Soc. Pet. ng. AIM , p 92-104, 1961.

[44] G.Strang, "On the Construction and Comparison of Difference Schemes", 4s",

[54] R.F.Warming and R.M.Beam, "Upwind Second Order Difference Schemes